Inter-American University of Puerto Rico
Advance Research and Innovative Experience for students
(ARIES)

TigreSAT
Science Report

Inter-American University of Puerto Rico
Advance Research and Innovative Experience for students
(ARIES)

Table of Contents

Bibliography 4

TigreSAT Team 2010-2011 5

Introduction 6

TigreSAT Mission Goal 6

Science Objectives 6

Technical Objectives 6

HASP TigreSAT Requirements 6

Data Preparation 7

Flight Analysis 8

Flight Trajectory 9

Phase 1 9

- Phase 1 Accelerometer 9
- Phase 1 Gyroscope 11
- Phase 1 Magnetometer 13
- Phase 1: Internal Temperature 17

Phase II 18

- Phase II Accelerometer 18
- Phase II Gyroscope 19
- Phase II Magnetometer 21

Attitude Determination (Kinematic Equations) 24

Conclusion 31

Appendix A Calibration Procedure 33

Inter-American University of Puerto Rico
Advance Research and Innovative Experience for students
(ARIES)

List of Figures

Figure 1: Data Process for Calibration..... 7
Figure 2: Dynamics division by phases 8
Figure 3: Complete flight path HASP 2010 (Aug 8, 2011) 9
Figure 4: Payload Acceleration in three axis during phase 1..... 10
Figure 5: Payload Acceleration in three axis during phase with temperature curve 1 11
Figure 6: Gyroscope X axis vs Time 11
Figure 7: Zoon into Gyroscope X axis vs Time..... 12
Figure 8: Gyroscope Y vs Time..... 12
Figure 9: Gyroscope Z axis vs Time..... 13
Figure 10: Magnetometer X axis vs Time 14
Figure 11: Magnetometer Z axis vs Time..... 14
Figure 12: Magnetometer Z axis vs Time..... 15
Figure 13: Field Intensity vs Time during Phase 1 16
Figure 14: 2010 Magnetic Field Intensity [2] 16
Figure 15: Temperature Profile during phase I..... 17
Figure 16: EQUIS 2011 Complete Flight Trajectory 18
Figure 17: Phase II Acceleration vs Time..... 19
Figure 18: Phase II Rotational Rate vs time 20
Figure 19: Magnetic Magnitude in X, Y and Z axis..... 22
Figure 20: q1 and q2 of the quaternion components..... 25
Figure 21: q2 and q3 of the quaternion components..... 25
Figure 22: Euler angles for data of HASP 2011 27
Figure 23: Kalman Filter process for converging on a true state vector..... 28
Figure 24: q1 and q2 of the filtered quaternion components 29
Figure 25: q3 and q4 of the filtered quaternion components 29
Figure 26: Euler Angles in for x, y and z axes..... 30

Bibliography

[1] Granger, D. (n.d.). *LSU Science Space Group*. Retrieved December 5, 2011, from Laspace LSU: http://laspace.lsu.edu/hasp/Flightinfo-2011.php

[2] geomag.models@noaa.gov. (2010, March 6). *NOAA national Geophysical Data Center*. Retrieved December 5, 2011, from The World magnetic model: http://ngdc.noaa.gov/geomag/WMM/DoDWMM.shtml

[3] Wertz, J. R. (1980). *Spacecraft Attitude Determination and Control* . D. Reidel.

[4] Wertz, J. R. (1999). *Space Mission Analysis and Design* . Space Technology Library.

[5] Garmin Corporation. (n.d.). Retrieved November 16, 2010, from Garmin Website: HYPERLINK "http://www8.garmin.com/aboutGPS/" 1

[6] Harris, M. B. (2006, September 25). Retrieved November 16, 2010, from HowStuffWorks.com: HYPERLINK "http://electronics.howstuffworks.com/gadgets/travel/gps.htm" http://electronics.howstuffworks.com/gadgets/travel/gps.htm

[7] Trimble. (n.d.). Retrieved November 16, 2010, from Trimble: HYPERLINK "http://www.trimble.com/gps/index.shtml" http://www.trimble.com/gps/index.shtml

[8] Corp., S. E. (n.d.). *MicroMag 3-Axis Magnetometer*. Retrieved February 11, 2011, from Sparkfun Electronics: http://www.sparkfun.com/products/244

[9] InvenSense. (2010, 03 30). ITG-3200 Product Specification Revision 1.4. Sunnyvale, CA, US.

[10] Corp., S. E. (n.d.). *One Wire Digital Temperature Sensor DS18B20* . Retrieved February 10, 2011, from Sparkfun Electronics: HYPERLINK "http://www.sparkfun.com/products/245" http://www.sparkfun.com/products/245

[11] Corp., S. E. (n.d.). *Triple Axis Accelerometer Breakout-SCA3000*. Retrieved February 10, 2011, from Sparkfun Electronics: HYPERLINK "http://www.sparkfun.com/products/8791" http://www.sparkfun.com/products/8791

[12] BIBLIOGRAPHY \l 1033 Torben Graversen, M. K. (2002). *Attitude Control system for AAU CubeSat (http://www.cubesat.auc.dk./dokumenter/acs_report.pdf).* 6: June.

[13] BIBLIOGRAPHY \l 1033 BIBLIOGRAPHY Greg Welch, G. B. (2006, July 24). *An Introduction to the Kalman Filter.* Retrieved June 20, 2011, from The Kalman Filter: http://www.cs.unc.edu/~welch/media/pdf/kalman_intro.pdf

Inter-American University of Puerto Rico
Advance Research and Innovative Experience for students
(ARIES)

TigreSAT Team 2010-2011

Javier I. Espinosa Acevedo- Team Student Leader

Undergraduate Electrical Engineering, Male, Hispanic

Mairim Nieves- Attitude Determination

Undergraduate Electrical Engineering, Female, Hispanic

Jorge Quiñones Arduino- Calibration and Control

Undergraduate Electrical Engineering, Male, Hispanic

Ana Espinal Mena- Attitude Determination System

Graduate Electrical Engineering, Female, Hispanic

Jose Almonte- Control and Data Analysis

Undergraduate Computer Engineering, Male, Hispanic

Natacha Nazario – Project Manager

Undergraduate Aviation Management, Female, Hispanic

Abdiany Rivera- Structure Design and Thermal Analysis

Undergraduate Mechanical Engineering, Male, Hispanic

Juan Rosado- Software

Undergraduate Computer Science, Male, Hispanic

Oscar Valle – Electrical Engineering

Undergraduate Electrical Engineering, Male, Hispanic

Inter-American University of Puerto Rico
Advance Research and Innovative Experience for students
(ARIES)

Introduction

TigreSAT Mission Goal

The goal of this project is to improve on the previous Attitude Determination System (ADS) developed by the EQUIS team by implementing it in a print circuit board. This new package will provide hands-on experience for the development of a CubeSat prototype by using standardized concepts to apply to the attitude determination of a body. The designing, developing and testing will serve as a stepping stone for a future CubeSat project. This experiment will serve as a test bed and training environment for the technology that could be used for the CubeSat project.

Science Objectives

- Obtain the platform body frame orientation with respect to the body fixed reference frame.

Technical Objectives

- Complete graphs and charts related to show the output of the different sensors as well as the translational and orientation motion of the cube.
- Develop a code to obtain data from the sensors and send it through telemetry.

HASP TigreSAT Requirements

Fields	**Design Requirements**
Electrical	30 @ 500mA (Max)
	CubeSat PCB Size
Software	1200 Baud
Mechanical	3kg Weight Limit
Fields	**Design Requirements**
Electrical	30 @ 500mA (Max)

Data Preparation

To analyze and interpret the data it is necessary to calibrate and convert the data in real values (e.g: μT, g, ^{o}/s). The following equations for the magnetometer, accelerometer and gyroscope were obtained through the calibration process:

Equation 1: Accelerometer X Axis = ((1.0032*(1.0030*(RAW)-32.6208)/1333)+0.02066)

Equation 2: Accelerometer Y Axis = ((1.0278*(0.9826*(RAW)+33.31)/1333)-0.0659)

Equation 3: Accelerometer Z Axis = ((1.0119*(0.9980*(RAW) -9.81211)/1333)-0.0243)

Equation 4: Gyroscope X Axis = ((1.0443*(0.9662439*(RAW)-26.018)/14.375)+2.44732)

Equation 5: Gyroscope Y Axis = ((0.9744* (1.0212*(RAW) + 0.5418)/14.375)-0.561)

Equation 6: Gyroscope Z Axis = ((0.9962* (0.9896*(RAW)+5.535)/14.375)-0.588447)

Equation 7: Magnetometer X Axis =((0.997*(RAW)-52.865))/31.24

Equation 8: Magnetometer Y Axis =((0.997*(RAW)-52.865))/31.24

Equation 9: Magnetometer Z Axis =((1.000015*(RAW)-101.32))/31.24)

The data was processed through a linear regression, then converted to real values and finally calibrated. Below is shown in **Figure 1** the process of this calibration:

Figure 1: Data Process for Calibration

For information and details of the calibration process and equations please refer to Appendix A. There it is explained the device used, procedures for calibration and a comparison between the not calibrated data vs. the calibrated data.

Flight Analysis

After obtaining the desired type of data, the flight data was divided into two phases. Phase 1 **Elevation** and Phase 2 **Flight** as shown in **Figure 2**. The division of the phases of the flight will allow better analysis because data resolution will be higher, therefore allowing a closer analysis at the graphs.

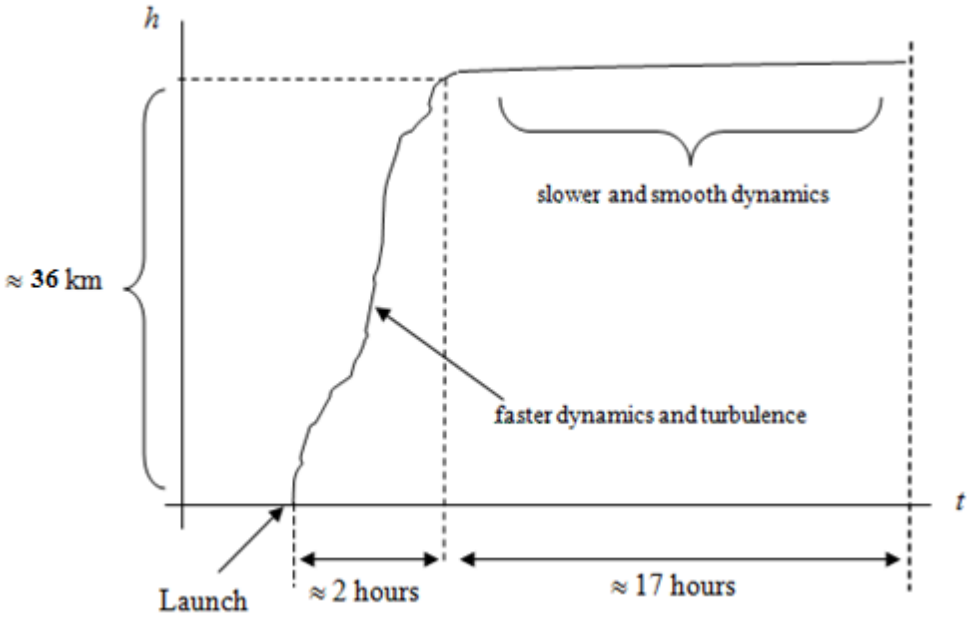

Figure 2: Dynamics division by phases

Phase 1 starts from the launch to the point that the altitude from the GPS data is not incrementing drastically (Reaches approx. 36km) this phase has faster dynamics and turbulence. Phase 2 starts right after phase 1 and last until the rest of the flight; this phase has slower and smoother dynamics.

Flight Trajectory

Through the LSU HASP site it was possible to obtain the image in Figure 3, it is possible to observe that the Zero Pressure Balloon started in New Mexico and ended Arizona. During this time a lot of data was obtained, therefore the data will be divided into phases to amplify the resolution in the charts.

Figure 3: Complete flight path HASP 2010 (Aug 8, 2011)

Phase 1

Through the LSU HASP site it is possible to obtain the GPS data of the payload, with this it was possible to identify when the phase 1 ends. Phase 1 ends about 2:23:36hrs after launch, according to the GPS data the Flight elevation started at 13:57:44GMT and reached an altitude of 123,070ft at 16:21:50GMT. In Figure 3 the blue arrow indicate where phase 1 finishes and phase 2 starts.

Phase 1 Accelerometer

Observing the graph in Figure 4 it can be notice that the accelerometer was able to record a 1g magnitude in the z axis and fairly zero in the other 2 axis until 1:34, then a sudden drop can be

observed, that last up to approximately 2:05hr by comparing the temperature graph it can be notice that at this same time the temperature was reducing reaching a minimum of approximately -14^{o}C; the sca3000 has a temperature range of -40^{o}C to 80^{o}C therefore temperature variation would not have caused this effect. The accelerometer was in an altitude of approximately 70,000ft at 15:14:40 GMT which is 1:17hrs after launch. At time 2.09hr the accelerometer continue sensing approximate 1g of gravitational acceleration as shown in Figure 4.

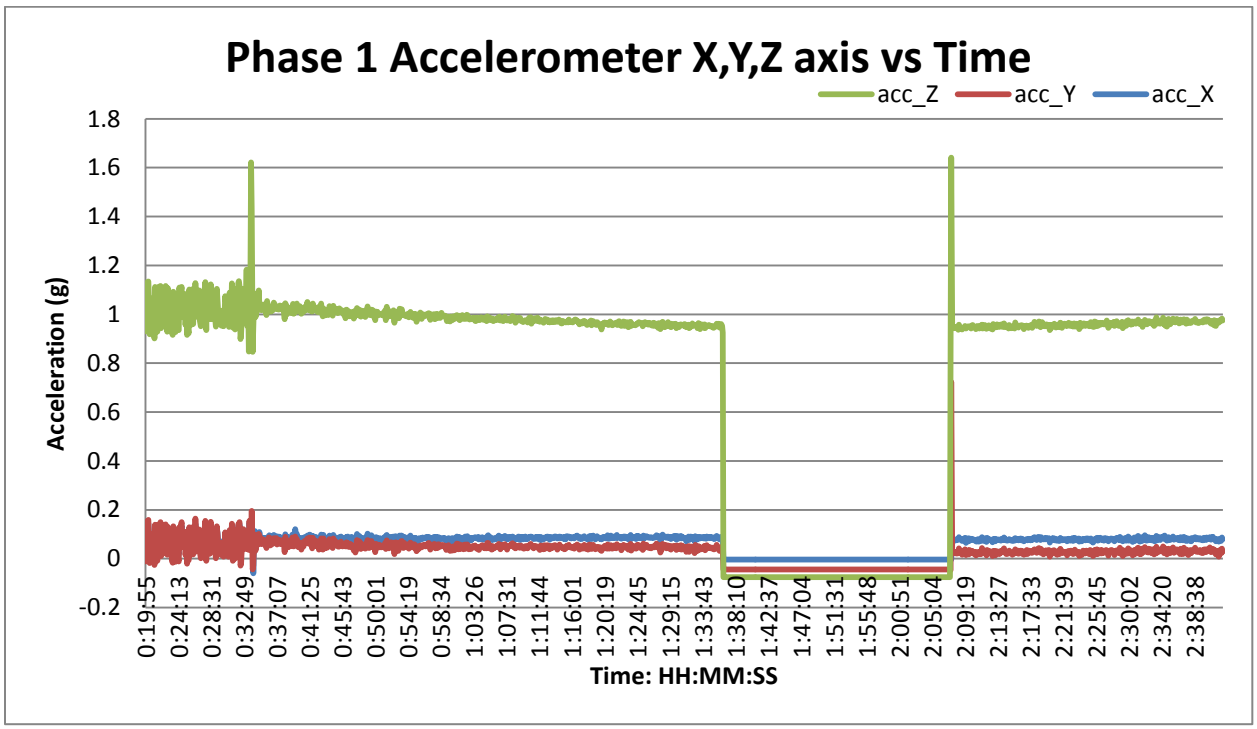

Figure 4: Payload Acceleration in three axis during phase 1

To better understand what happened during the time of 1:38 to 2:09 in **Figure 5** the payload acceleration in X, Y and Z was plotted with the temperature curve over it to allow a visual understanding of the event. During the period of low acceleration magnitude in the Z axis the internal temperature was approximate -14^{o}C and then the temperature raising to 20^{o}C. The z axis was pointing in the vertical direction and the other two axis where perpendicular to the Z axis, therefore it expected that the z axis will be the component with most magnitude. Accordingly during the first phase there were no fast dynamics except for the event from 1:38 to 2:09.

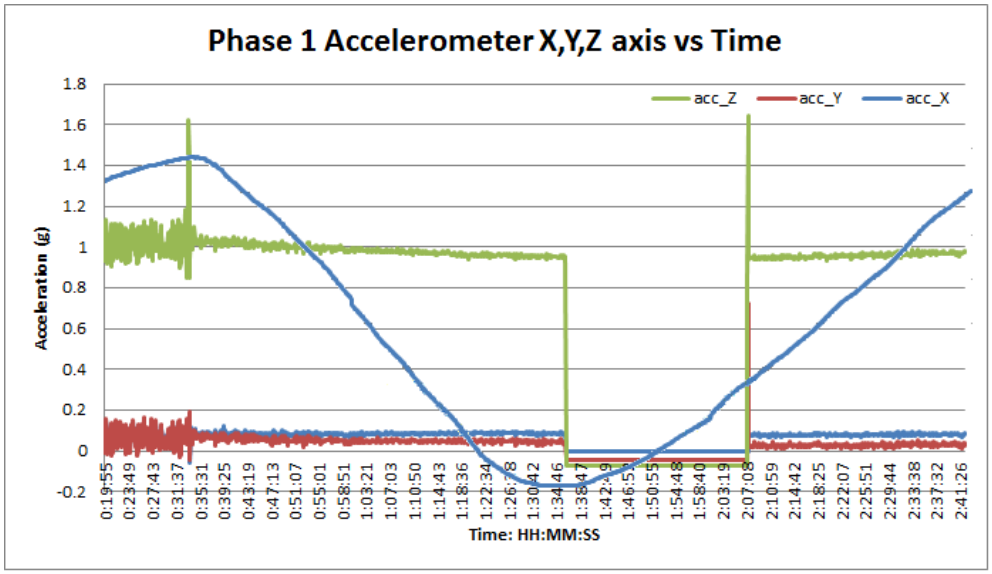

Figure 5: Payload Acceleration in three axis during phase with temperature curve 1

Phase 1 Gyroscope

The gyroscope sensor will give the rotational rate of the payload during the flight in three axes, taking into account that the z axis is in the vertical direction. Accordingly to the data of the phase 1 plotted in **Figure 6** it is possible to observe that in the x axis the gyroscope was rotating at a slow and varying rate in the counterclockwise direction in the range of -4 to 2.5 degrees per second. In the data it can be observe that there is a spike that reaches a magnitude of approximate 8.5°/s which is also notice in the Y and Z axis.

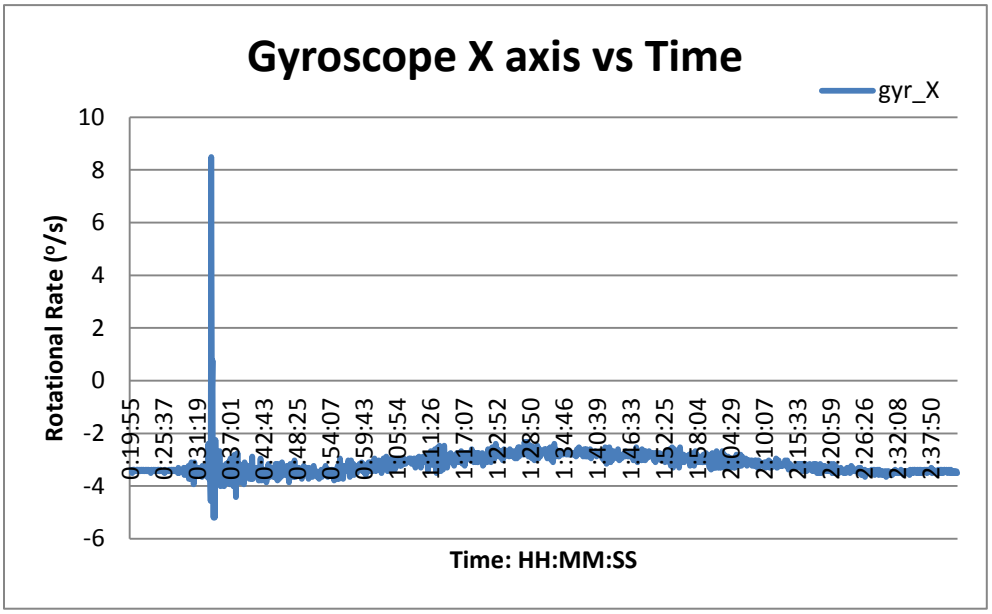

Figure 6: Gyroscope X axis vs Time

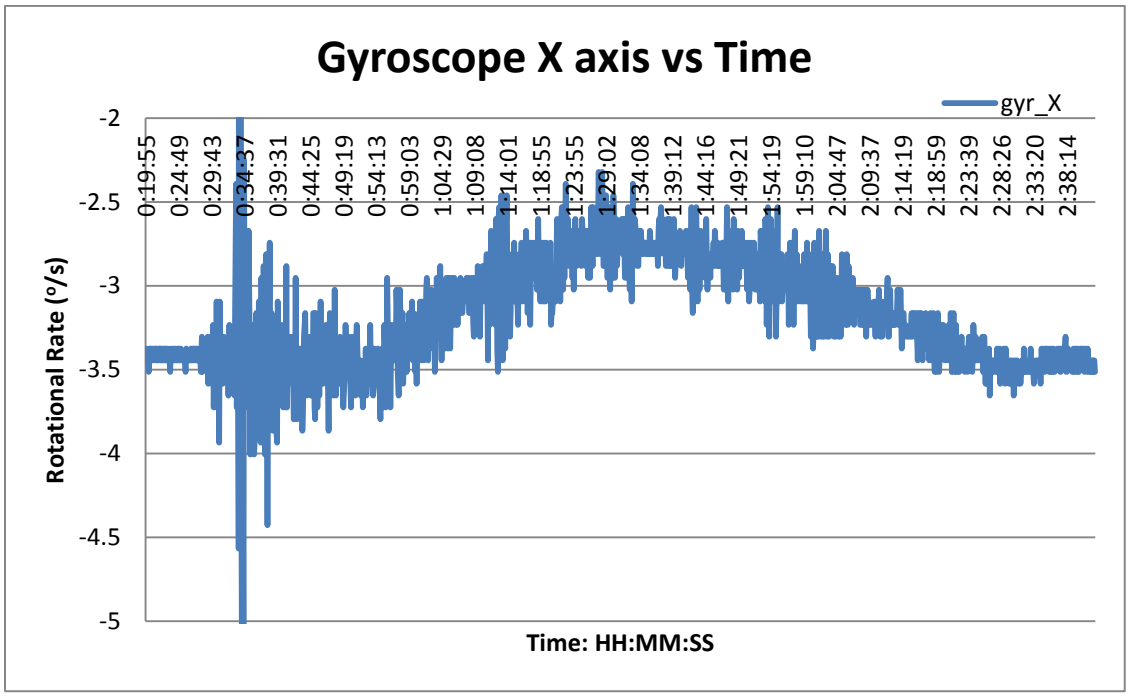

Figure 7: Zoon into Gyroscope X axis vs Time

Figure 7 is a zoom to the X axis since its rotational rate maintained in the range of -2.5 to 4 degrees per second. It can be noticed that after 1:10hrs the rotational rate reduced to approximate 2.75 degrees per second. In the Z axis of the gyroscopic sensor it is possible to determine that the payload was not having much rotational rate; therefore maintaining in approximate zero to one degree per second as shown in **Figure 8**.

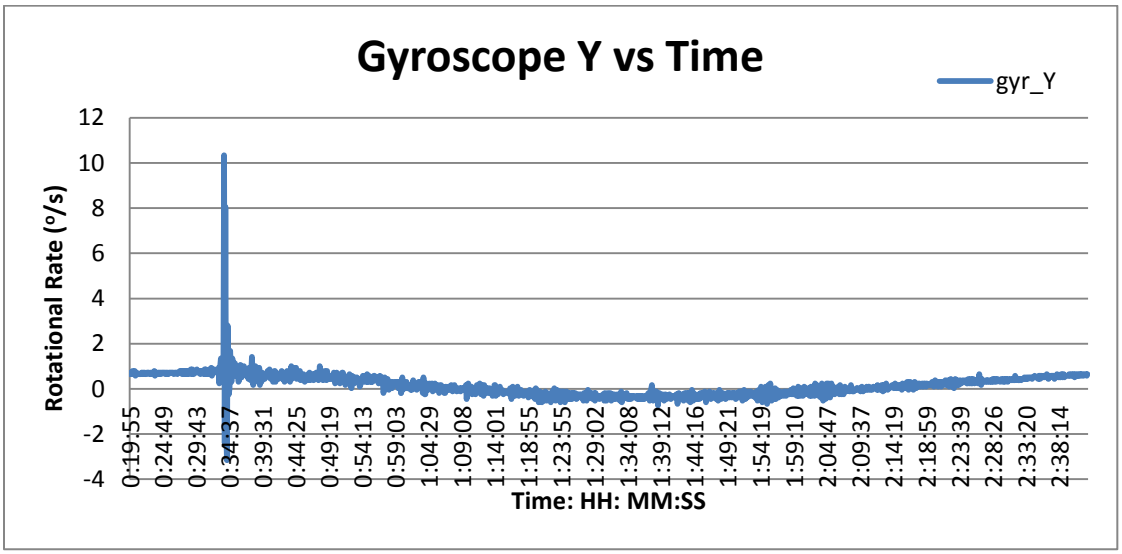

Figure 8: Gyroscope Y vs Time

During the flight the z axis of the gyroscope showed significant rotations. According to Figure 9 the payload maintained rotating CCW (negative rotations), during the first hour and then started rotating CW in a range of 0-5 degrees per second. Several spikes reached 10 and 13 degrees per seconds.

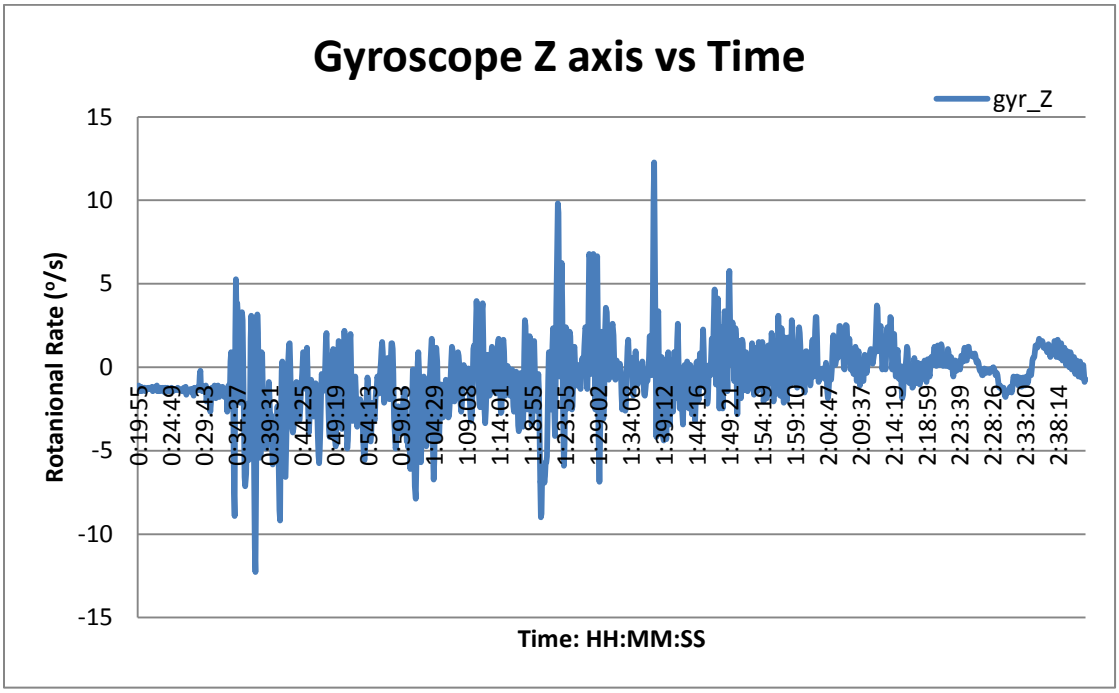

Figure 9: Gyroscope Z axis vs Time

Phase 1 Magnetometer

Data analysis using the magnetic field can become very complex, the magnetic field properties of the earth are in a constant change. In Figure 14-16 it is possible to observe the magnitude recorded on each axis of the Micromag3 sensor during phase I of the flight. It is possible to observe that in the x axis the magnitude recorded varied from -25uT to 25uT. The Y axis varied from -30uT to 25uT and the Z axis remained fairly constant approximately 51uT. These ranges in the data can be observed on **Figures10, 11, 12.**

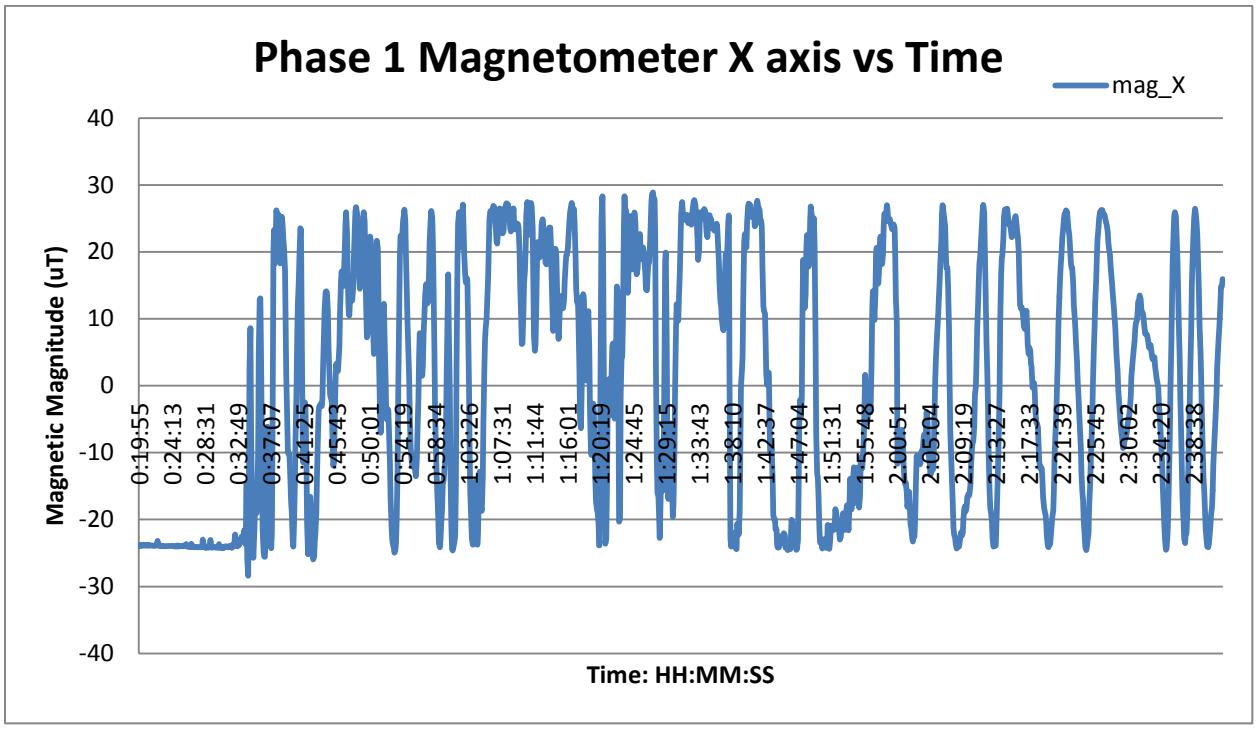

Figure 10: Magnetometer X axis vs Time

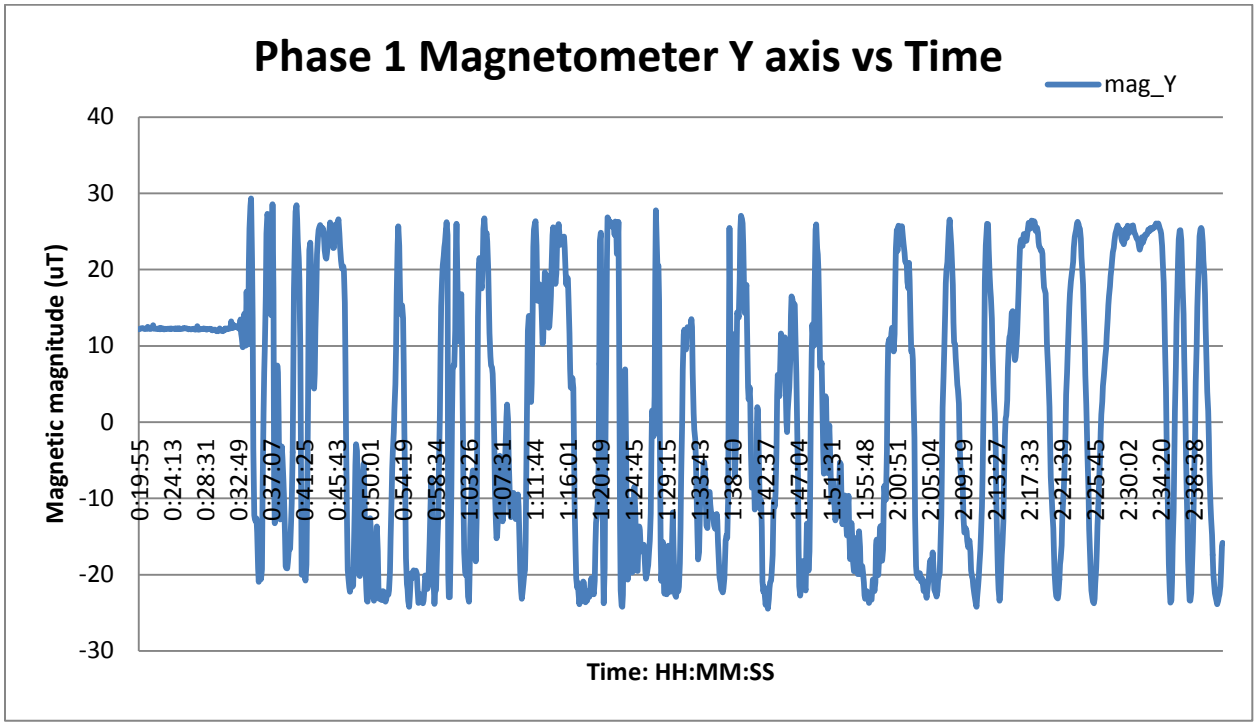

Figure 11: Magnetometer Z axis vs Time

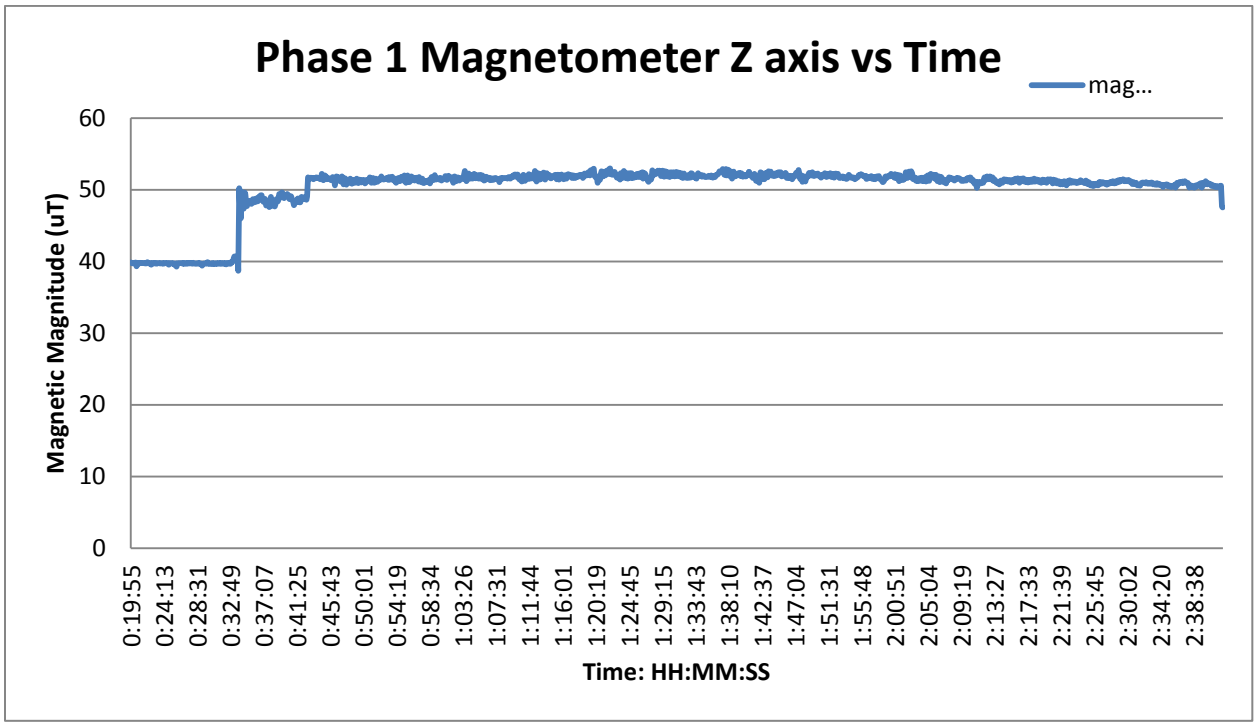

Figure 12: Magnetometer Z axis vs Time

Observing the data it can be possible to understand the resolution and range of the data; therefore, through the data analysis it could be possible to determine if the sensor would be appropriate for an attitude determination system. To understand the data it was converted to field intensities (F) with **Equation 1**.

Equation 10: $$F = \sqrt{X^2 + Y^2 + Z^2}$$

Where:
F: Total Field Intensity
X: x axis of magnetometer
Y: y axis of magnetometer
Z: z axis of magnetometer

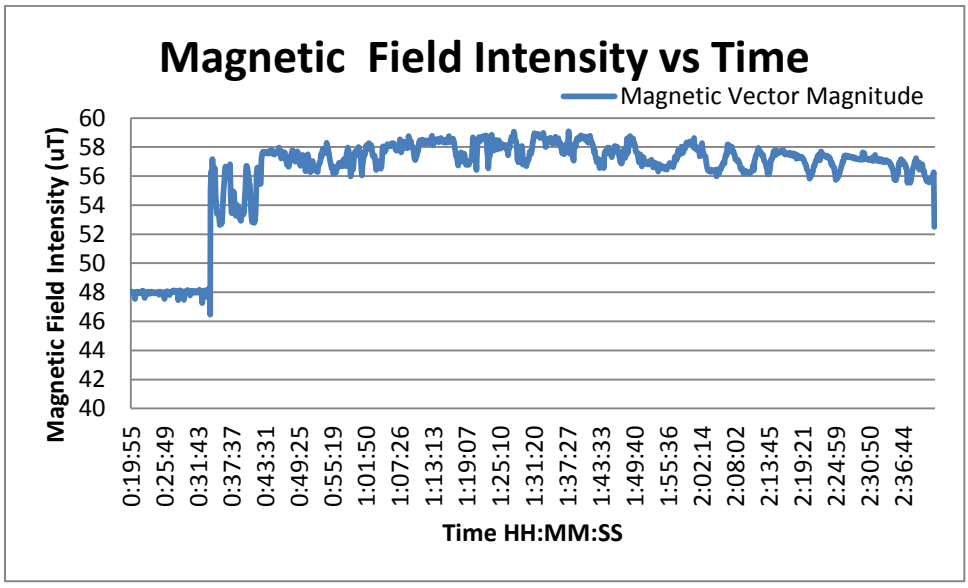

Figure 13: Field Intensity vs Time during Phase 1

The **Figure 13** permits an understanding that the field intensity was in the range of 48 to 61uT. Since we know it was in the United States where the flight took place it is possible to observe that the payload headed north during the flight to some degree. In **Figure 14** it is possible to observe the earth magnetic field intensity over the US, it can be observe that the field intensity increases more in the north direction. A small square represents where New Mexico will be located on the map, permitting to identify the field intensities of the area.

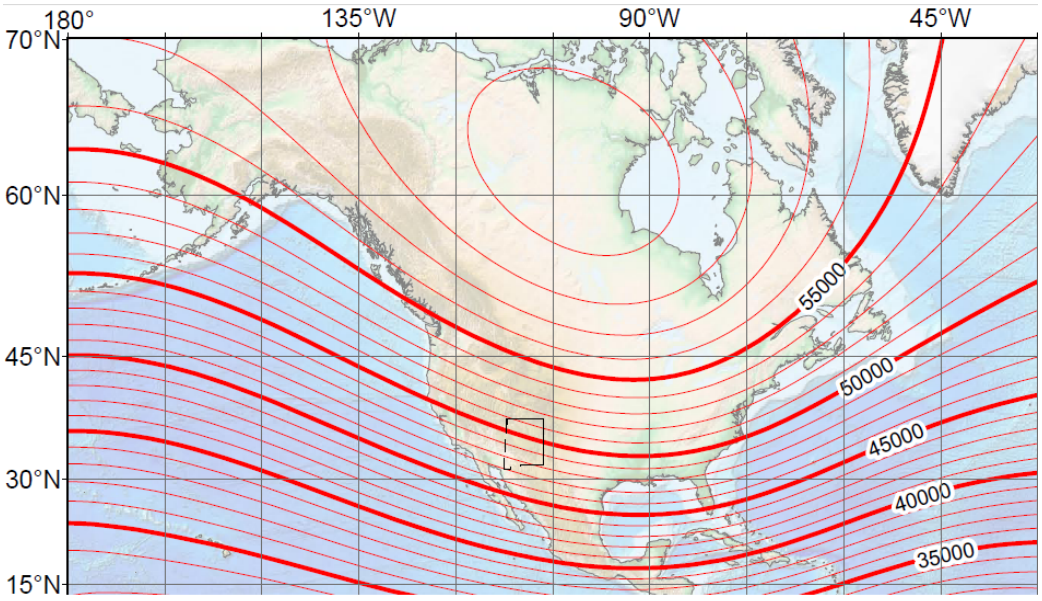

Figure 14: 2010 Magnetic Field Intensity [2]

Phase 1: Internal Temperature

During the first phase of the flight the internal temperature varied, it first went from 21°C to 24°C then it slowly decreased to a value of -14°C and the increased. The phase one finished with a temperature of 20°C. Allowing us to acknowledge that the internal temperature in the payload remained within the establish parameters during the first phase.

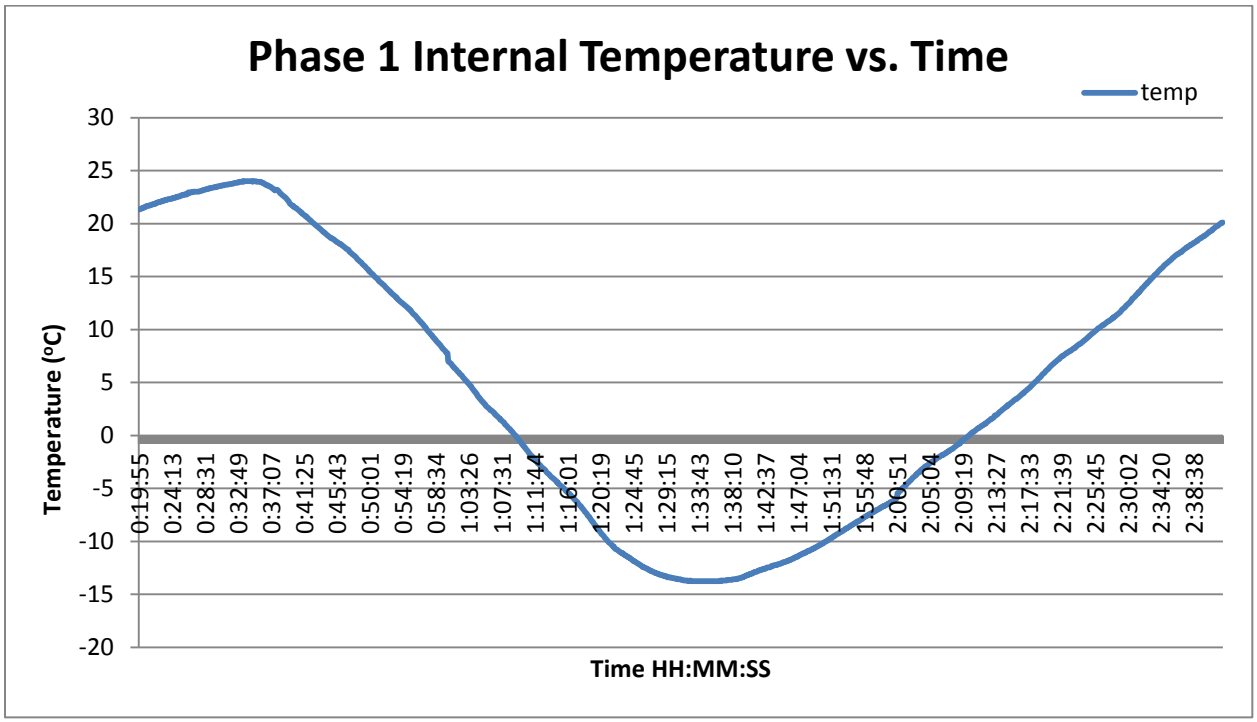

Figure 15: Temperature Profile during phase I

Phase II

The phase II is the longest section of the flight it lasts approximately for 14:43hrs, in **Figure 16** it can be observe the location of where the first phase ended and where phase II started. This phase finishes where the payload reaches its final location mark with the purple "F" located in Arizona with approximately 16:85hr of total flight time.

Figure 16: EQUIS 2011 Complete Flight Trajectory

Phase II Accelerometer

It was possible to obtain the acceleration of the payload through the period of the flight. During this phase of approximately 14:43hrs of flight, data was obtained and plotted as shown in the **Figure 17**. In the plot we have all three axis, it can be observe that the accelerometer measured 1g (earth's gravitational acceleration) in the Z axis and closely to zero the Y and X axis. This is known to be true since the Z axis is in the vertical direction. It can be observed that the gravitational acceleration changes as the distance increases and becomes stable when it is in the second phase of flight, until the descend of the HASP platform at approximately 14:50hr when the measures were affected by the extremely change in gravitational acceleration.

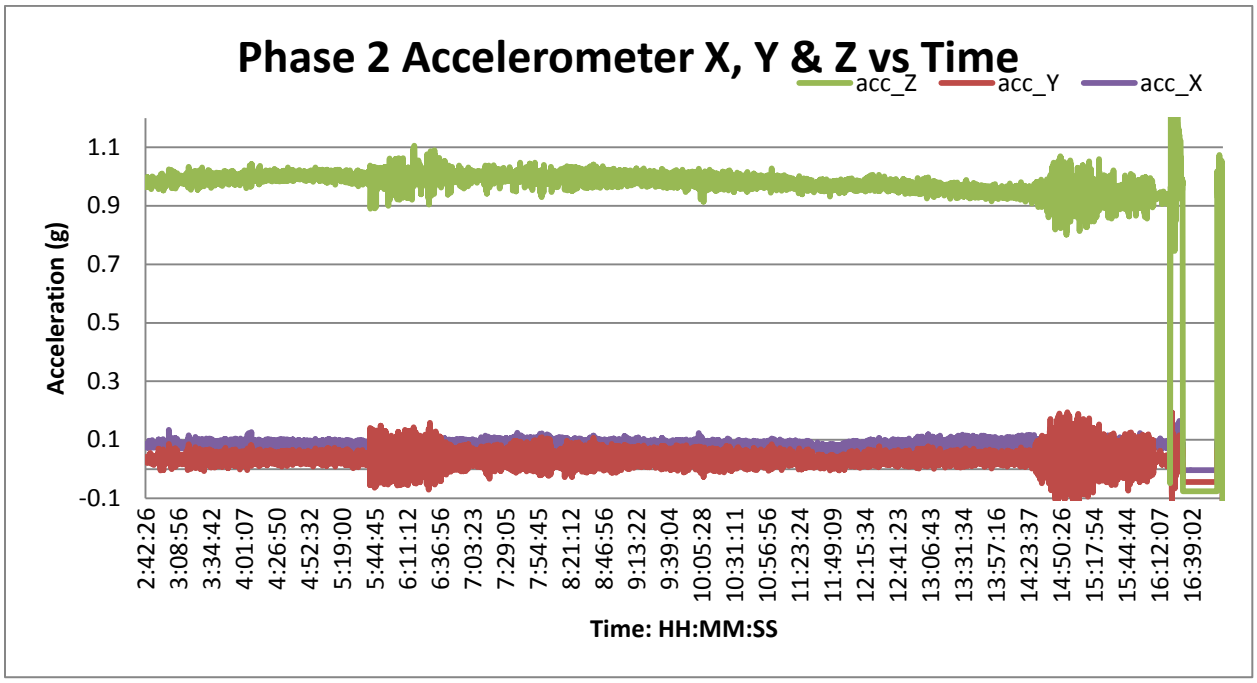

Figure 17: Phase II Acceleration vs Time

Phase II Gyroscope

During the phase II, by observing **Figure 18 and 19**, it is possible to notice that the rotational rate did not varied significantly from -2°/s to -5°/s this shows a slightly rotational rate on the pitch and yaw motion rather than roll motion. Therefore this information allows understanding how the balloon moves through phase II of the flight and being able to realize that the HASP platform remain nearly immobile in the second phase of the flight. Through the analysis of this data it can be observed that the rotational rate increases drastically to approximately 130 °/s when the HASP platform begins to descend at 16:15hr as shows in **Figure 19.**

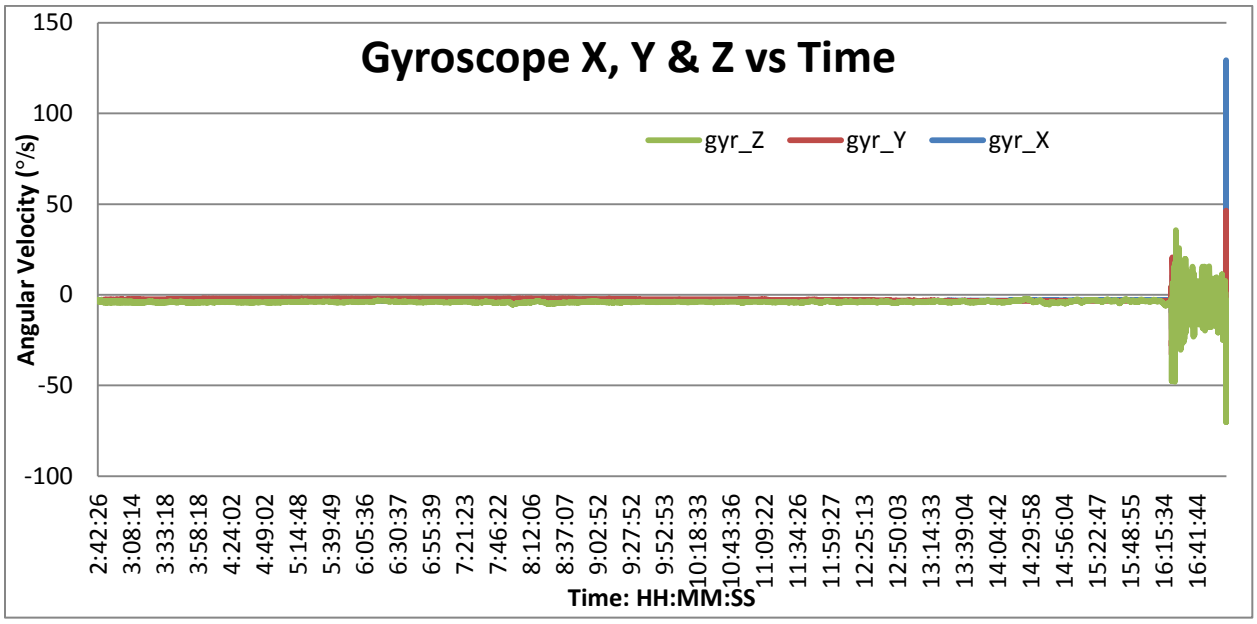

Figure 18: Phase II Rotational Rate vs time

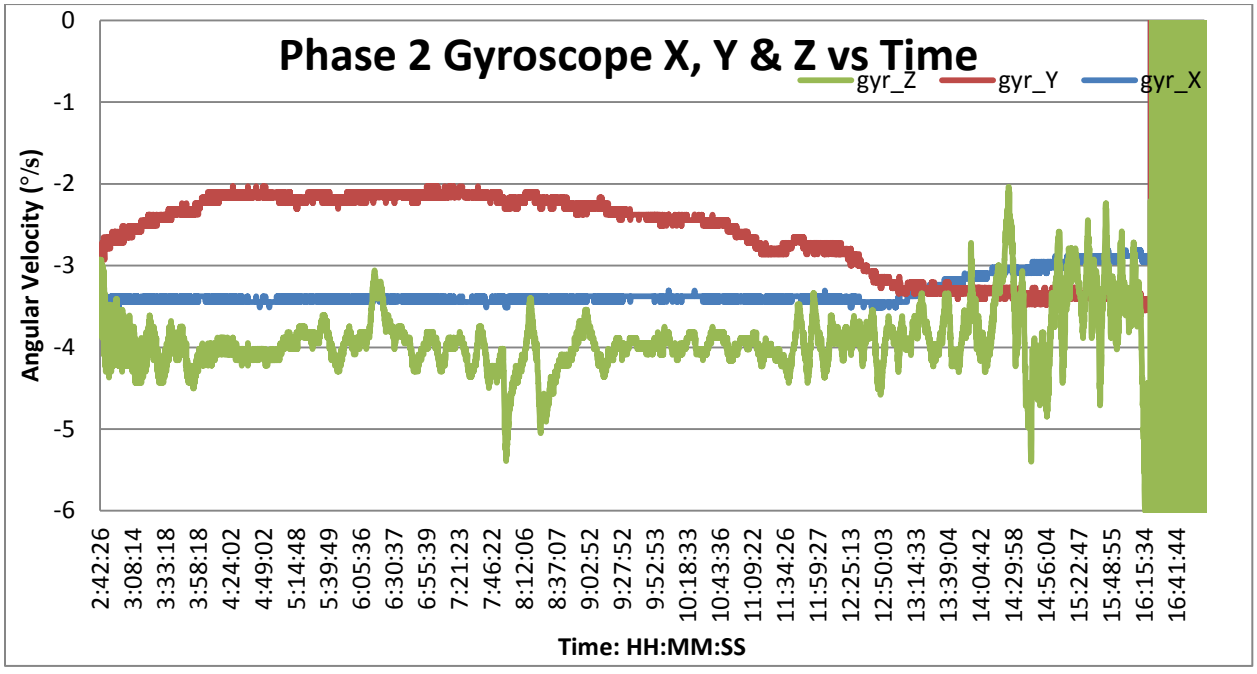

Figure 19: Phase II Zoom Rotational Rate vs time

Phase II Magnetometer

In **Figure 20 and Figure 21** the variations of the magnetic field were in the same range of that in of Phase I. In comparison with phase 1 the variations were much less in the phase II due to the achieved stability of the flight. The data obtained from magnetometer provides a great deal of information because it shows that in the Y and Z axis, the pitch and yaw motion of the balloon is moving at a higher rate. The roll motion is so small that it does not cause a change in the measurement of the Z axis in the magnetometer. Furthermore the magnitudes obtained are converted to Field Intensity of allow a better understanding of the data.

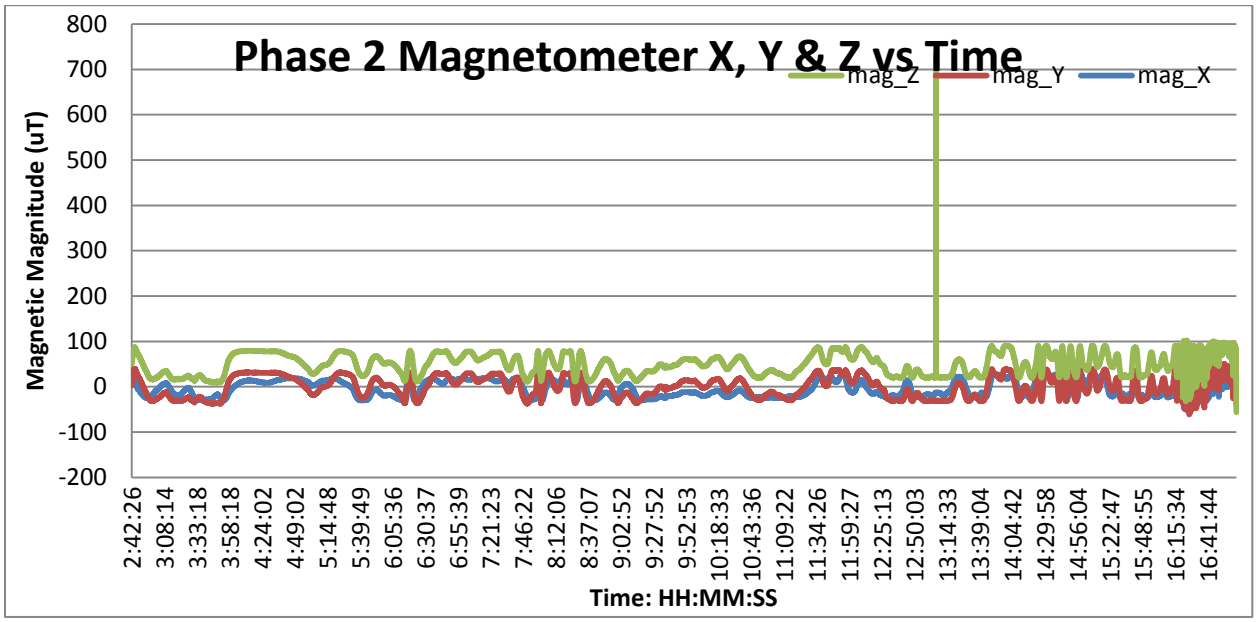

Figure 20: Magnetic Magnitude in X, Y and Z axis

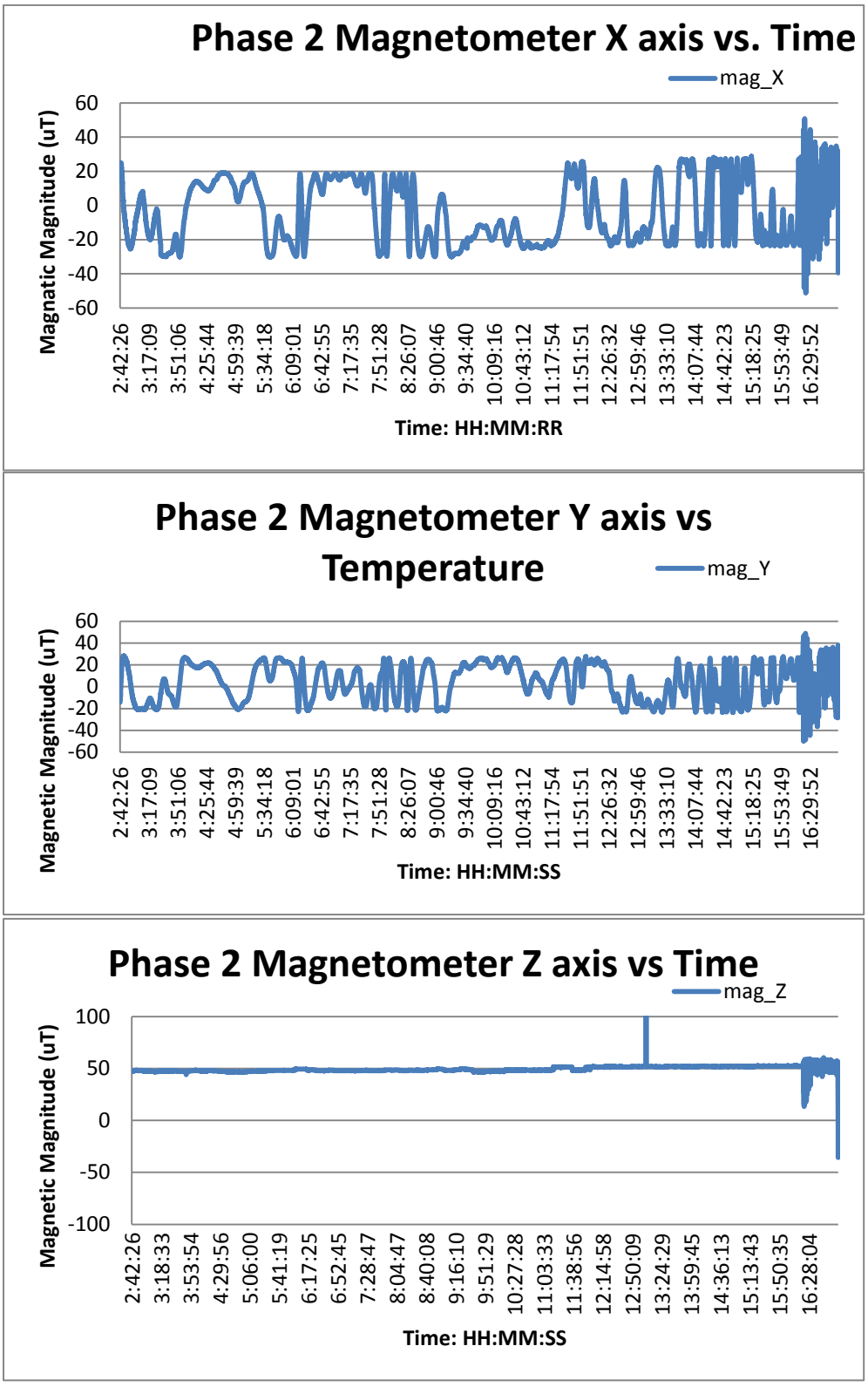

Figure 19: Magnetic Magnitude in X, Y and Z axis

With Equation 1 shown again for convenience

$$F = \sqrt{X^2 + Y^2 + Z^2}$$

It is possible to observe the field intensity variation throughout the flight in **Figure 22** the variation were in the range of 65uT to 49uT, this can allow us to identify more area where the payload was exposed to, all through there are some specific values at approximately 13:12hr as shows in **Figure 23** were the magnetometer measured approximately 764 uT . This could be caused by Electromagnetic Interference by the other payloads or a unknown source of interference.

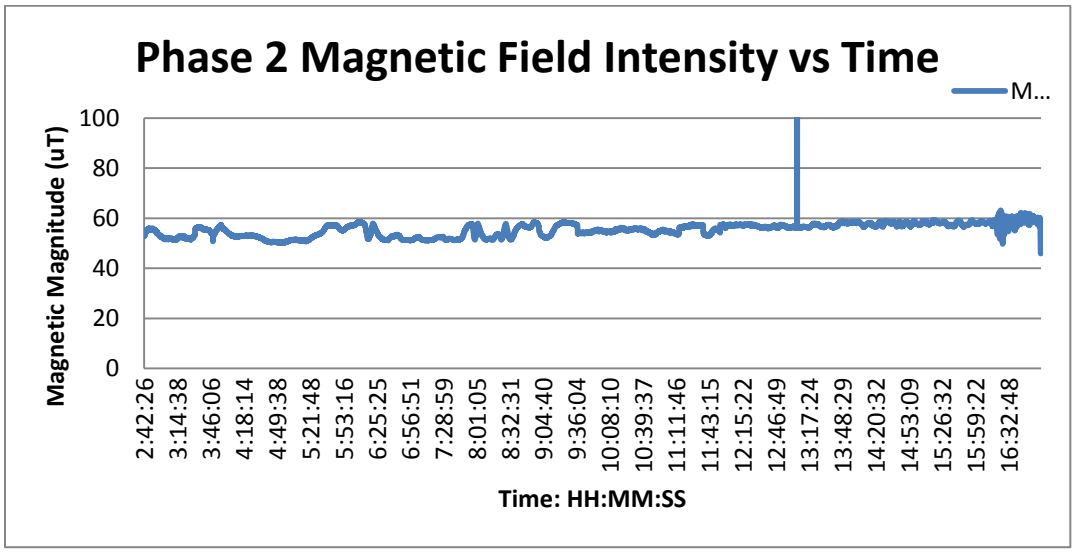

Figure 22: Field Intensity vs Time

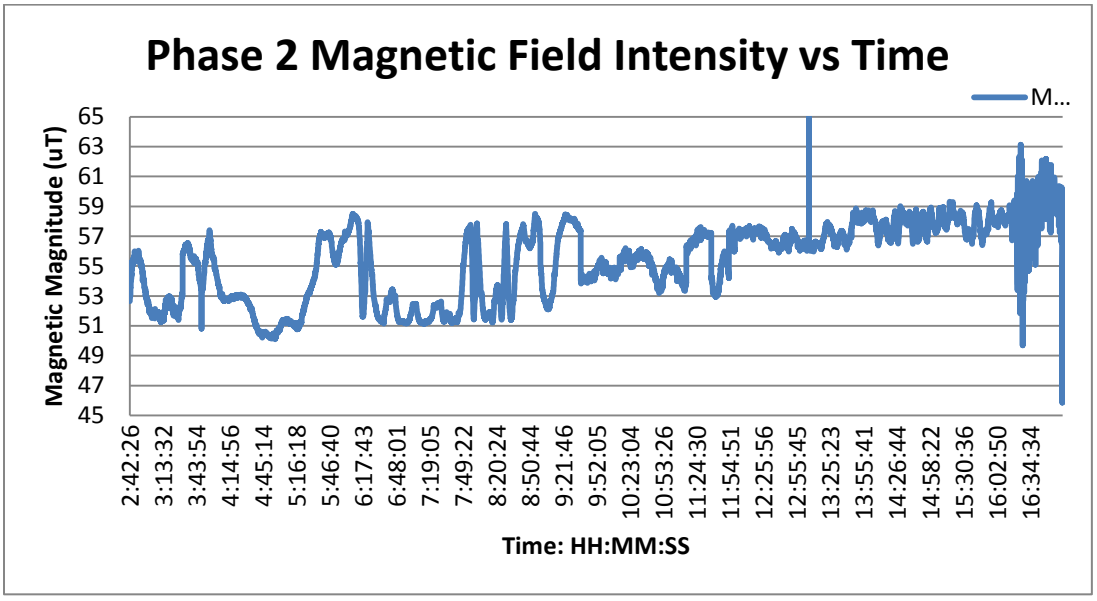

Figure 23: Zoom Field Intensity vs Time

Attitude Determination (Kinematic Equations)

The attitude determination system will be using the accelerometer, magnetometer and gyroscope data to perform a calculation which will describe the rotation and orientation of the platform during flight. For instance, let use the gyroscope data to describe the angular velocity. The following kinematic equation describes the rotation of the body about its center of mass. This equation is described in terms of the quaternion and angular velocity. The angular velocity is obtained from an IMU located in the body of the HASP payload. The kinematic equation can be written as,

$$\frac{dq}{dt} = \begin{bmatrix} 0 & -\varpi_1 & -\varpi_2 & -\varpi_3 \\ \varpi_1 & 0 & \varpi_3 & -\varpi_2 \\ \varpi_2 & -\varpi_3 & 0 & -\varpi_1 \\ \varpi_3 & \varpi_2 & \varpi_1 & 0 \end{bmatrix} \begin{bmatrix} q_1 \\ q_2 \\ q_3 \\ q_4 \end{bmatrix} \quad (1)$$

where $\vec{\varpi}$ is the angular velocity of the body, and $q = \vec{q} + q_4$. q is the quaternion explaining the orientation of the HASP platform, and q_4 is the magnitude of the rotation of the body. The calibrated data of the gyroscope for the HASP 2010 payload was substituted into equation (1), and it is assumed that the initial quaternion is,

$$q_0 = 0\hat{\imath} + 0\hat{\jmath} + 0\hat{k} + 1$$

A quaternion is a four component object with a three vector part and a scalar part. For this case the scalar part is 1. The quaternion are used instead of Euler angles to represent rotation due to the simplicity of calculation. In addition they are simpler to compose and avoid the problem of gimbal lock.

Using a MatLab code to integrate equation (1) with a real data taken from HASP 2011 in **Figure 20** and **Figure 21** shows the quaternion obtained from the integration procedure.

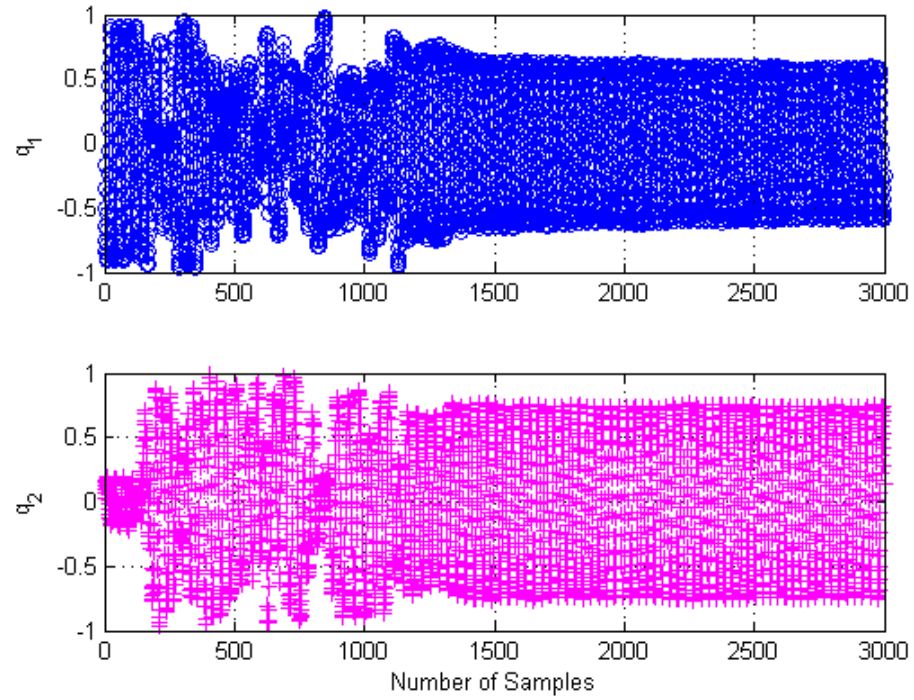

Figure 20: q1 and q2 of the quaternion components

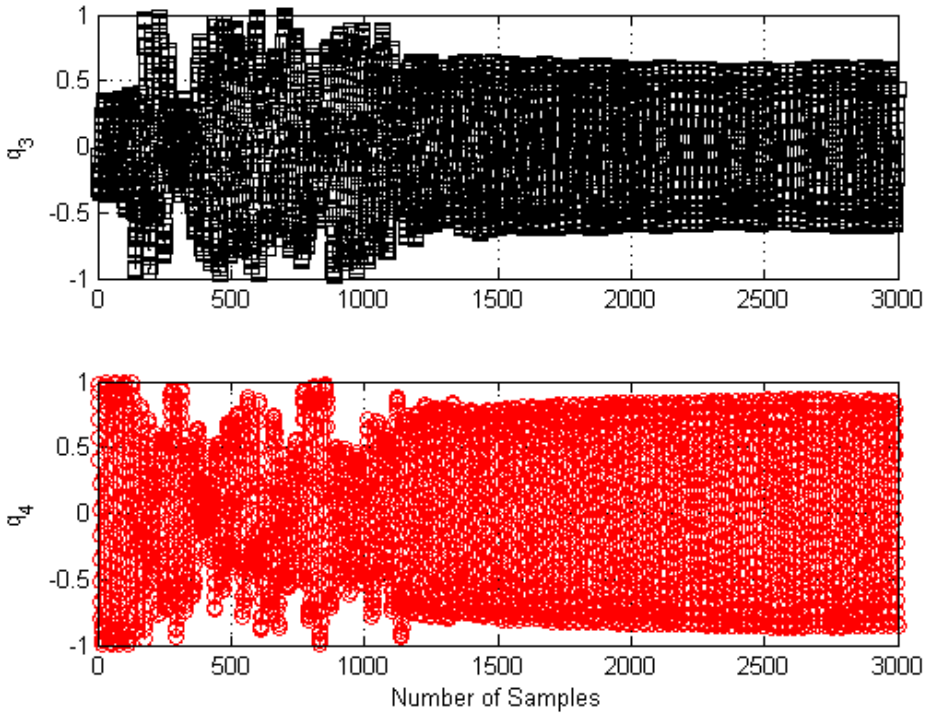

Figure 21: q2 and q3 of the quaternion components

As shown for the first 1250 samples is where the HASP was getting altitude and after this point is where it started to have some stabilization, for this range is called Phase 1.This data coincide with the time of two and half hours where after this point the HASP trajectory is more horizontal, for this one is called Phase 2.

After is performed the rotation using quaternion is then transformed into Euler Angles. The Euler angles provide a better understanding of the satellite motion. The transformation from quaternion into Euler angles can be written as,

$$\sin\theta = 2q_4q_2 - 2q_1q_3 \quad \text{(2a)}$$

$$\tan\varphi = \frac{2q_2q_3+2q_4q_1}{2q_4^2+2q_3^2-1} \quad \text{(2b)}$$

$$\tan\psi = \frac{2q_1q_2+2q_4q_3}{2q_4^2+2q_1^2-1} \quad \text{(2c)}$$

θ is the pitch angle, φ is the roll angle, and ψ is the yaw angle. The roll, pitch, and yaw angles describes the rotation about the x, y, and z axis of the payload, respectively. Using these equations, **Figure 22** shows the angle motion of the payload. In **Figure 22**, the pitch angle shows that the payload base was rotating from -90 to 90 degrees about the y axis. The roll motion shows a very similar rotation with the yaw axis. For the x and z axis did not occurred a decrease in rotation during the phase 1.

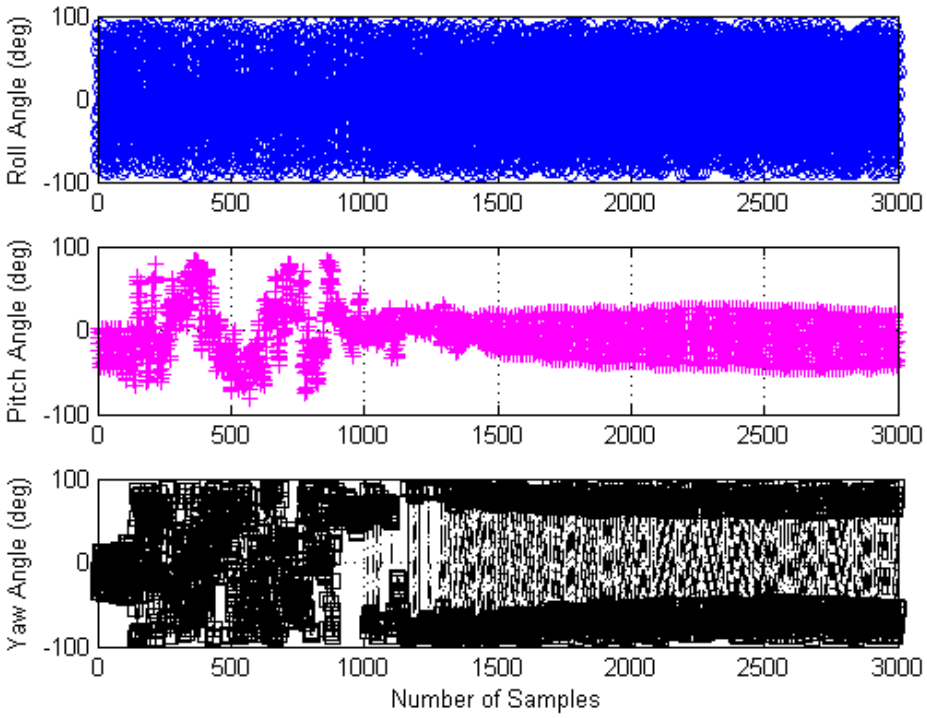

Figure 22: Euler angles for data of HASP 2011

The Kalman filter is an algorithm which uses a system dynamic model used to process noisy data retrieved from sensors measurements as an example, to accurately predict an attitude motion of an object in movement. It uses a recursive mathematical model to estimate the state of a process while minimizing any error in the system. The purpose is to force the measured and estimated values for the filter's state to converge and for the difference between the estimate and actual state, to be minimized. The Kalman filter can be represented by the following equation,

$$\bar{X}_k = K_k Z_k + (1 - K_k)\bar{X}_{k-1} \quad (3)$$

where,

$$\bar{X}_k = current\ estimation K_k = Kalman\ gain Z_k = measured\ value \bar{X}_{k-1} = previous\ estimation$$

and the k subscript are states or in state vectors,

$$x(k) = Ax(k-1) + Bu(k-1) P(k) = AP(k-1)A' + Q$$

where P is the initial value of covariance and Q is the process noise covariance.

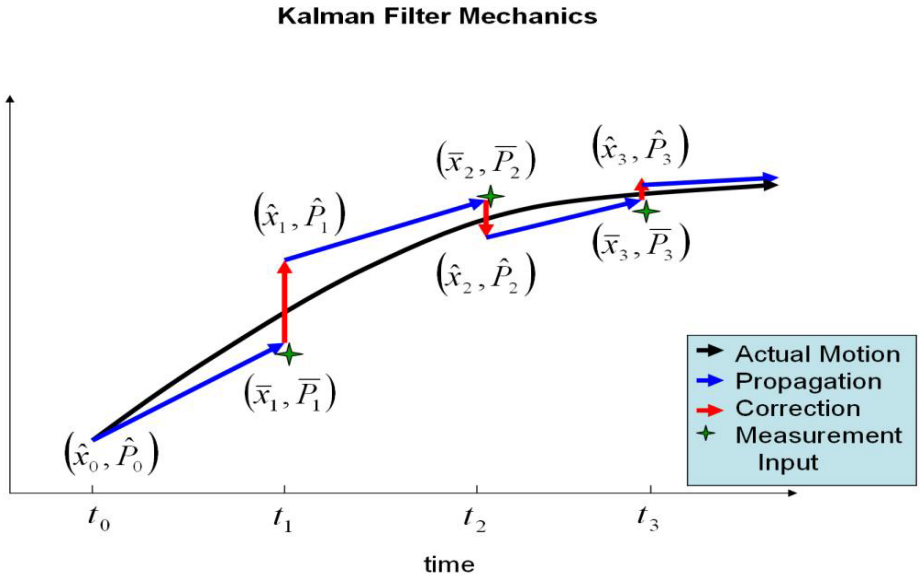

Figure 23: Kalman Filter process for converging on a true state vector

Figure 23 shows a graph representation of what the Kalman Filter perform. The y-axis represent the position and the x-axis the time. Each new step will try to correct its error using the previous value. The Kalman Filter can be used together with the Gauss-Newton method. The Gauss-Newton method is used to solve non-linear least squares problems. This method uses $B_k = J_k^T J_k$ where J_k is the Jacobian matrix. Its advantage is that for a second derivative which can be difficult to compute is not required.

Using the data from HASP 2011 was implemented the Kalman Filter as shown in **Figure 24** and **Figure 25**. The data presented of the quaternion is normalized. Each time a conversion from Euler Angles to quaternion and in reverse operation to the result can be added some error. Because of this error that can be added the quaternion are normalized as shown in the figures below.

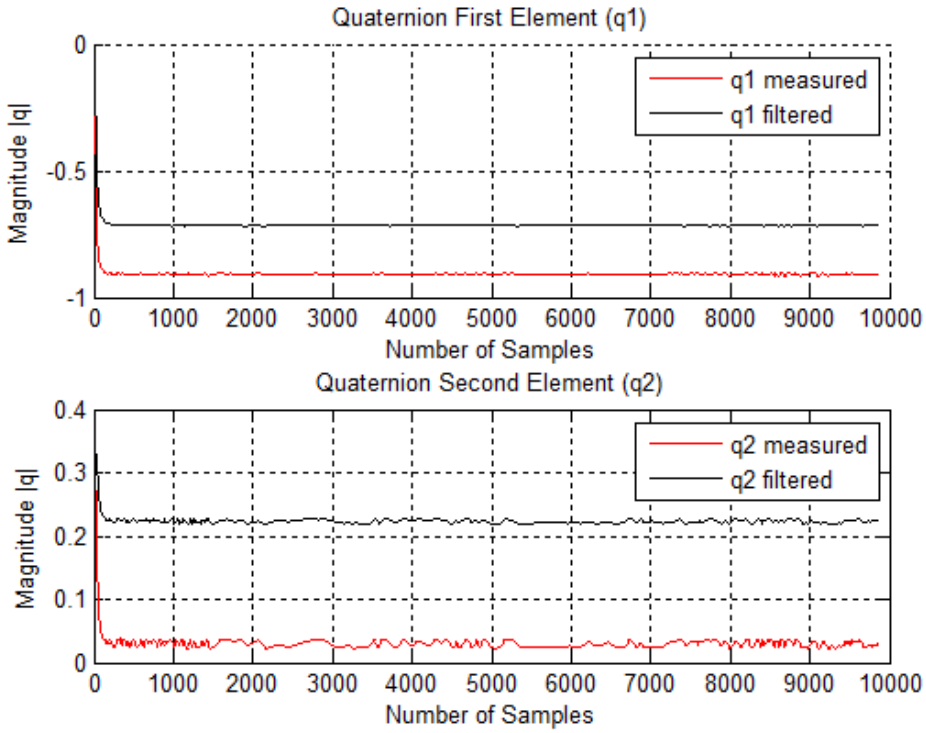

Figure 24: q1 and q2 of the filtered quaternion components

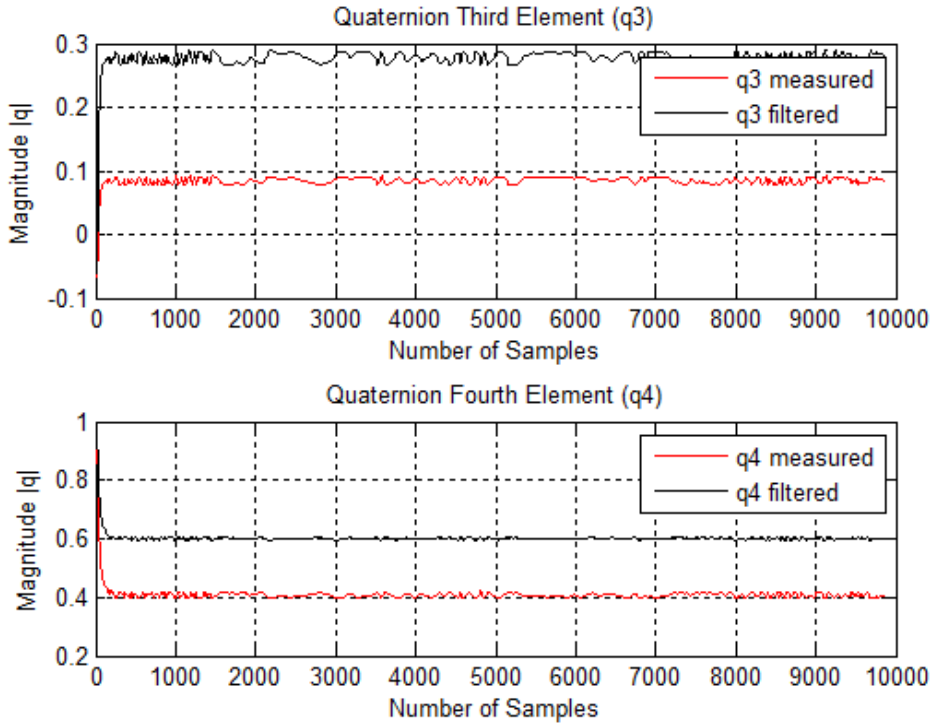

Figure 25: q3 and q4 of the filtered quaternion components

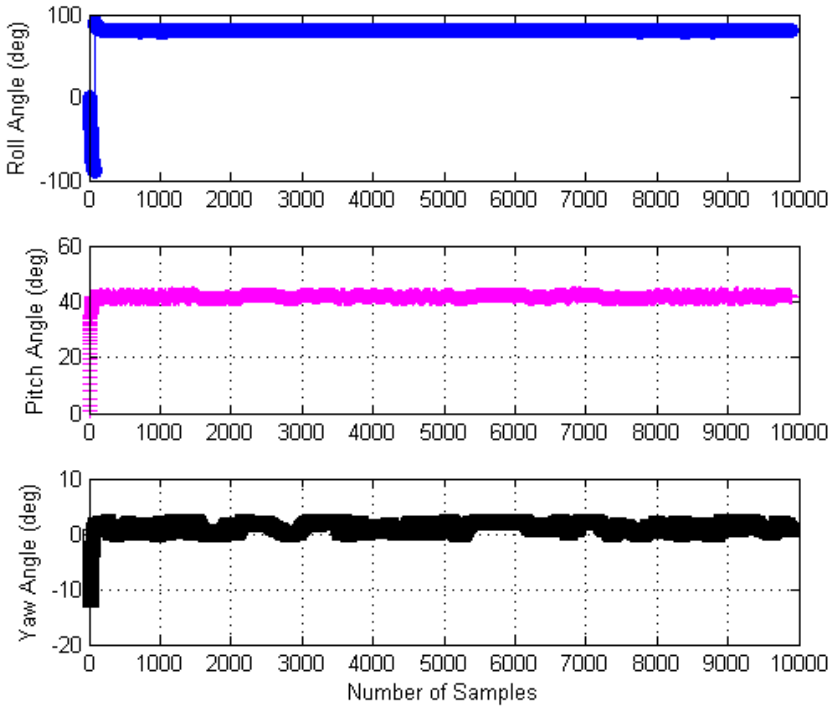

Figure 26: Euler Angles in for x, y and z axes.

Conclusion

The development of this payload allowed us to continue to learn about the development of an attitude determination system. The experiment required to develop a similar ADS but with a Global Positioning System (GPS) and by following the PC/140 standards. The ADS was implemented following the PC/104 dimensions requirements and using surface mount technologies. It was possible to go process of going through, PDR, CDR, FRR, Integration Plan, FLOP and Final Report. The development and implementation of an attitude determination system was completed, tested and flown on September 2011. After flight it was possible to analyze the data in a graphical format and obtains the characteristic of the behavior of the TigreSat payload through the Attitude Determination System (ADS), thus allowing us to observe the range of the data, the resolution, behavior and variations throughout the flight. It is necessary to understand that a graphical analysis can help understand the behavior of the payload throughout the flight. It was possible to notice through the data that phase I had faster dynamics and that the phase II was slower, as expected.

A situation occurred during the implementation with the Lassen IQ GPS on the PC/104 ADS board, at the end of testing and changes the Atmega328P did not have sufficient memory to obtain the NMEA GGA data, therefore the GPS was going to be used to actualized the Real Time Clock (RTC), also that did not occurred throughout the flight but it was possible to keep the time with the timer that was initially implemented.

Without the GPS data, the measurements of the Earth's magnetic field, gravitational field and angular momentum from the IMU sensors, which consisted of accelerometer, magnetometer, and gyroscope were successfully determined and transformed to quaternions to obtain the orientation and attitude of the payload similarly to that of the EQUIS payload. The implementation of the Kalman filter algorithm in the quaternions, permitted to obtain data signal with less noise and higher precision; therefore increasing the reliability of our attitude estimation. These quaternions were transformed to Euler angles consisting of roll, pitch, and yaw angles. The results showed that the transition from Euler angles to quaternion did not affect the final results. When

comparing the motion in roll, pitch, and yaw, the roll motion shows a very similar rotation, but there is a point in time that the payload is close to 5 degrees. This means that the wind is causing the base to rotate a lot about the x and z axis while the y axis shows a bounded motion. According to the data, the TigreSat payload had slower dynamics throughout the flight than the EQUIS payload.

The quaternion graphs which contain the quaternion components separately showed a bias with respect to the measured and filtered quaternion values. This is due because most of the gyroscope has a bias offset also known as the null voltage and is the measured voltage when the gyro is not rotating about its axis. The gyro output voltage measurements above the bias offset indicate rotation in one direction, while voltage measurements below the bias offset indicate rotation in the opposite direction.

The Euler Angles for x, y and z axis shows the output when is transformed from the quaternion back to Euler Angles. Although the data sample is every each 6 seconds at some point between the 80 and 81 samples for the roll axis there were not decimal values. Because of this, you can see a straight line that goes up suddenly. When is analyzed the Euler Angles versus the quaternion is found some stability for of rotation for each axis. The roll axis is where less perturbation had while the yaw axis was rotating left to right about 5 degrees. This makes sense because if the HASP payload is in a balloon you do not expect much rotation for the other angles as for the yaw.

Inter-American University of Puerto Rico
Advance Research and Innovative Experience for students
(ARIES)

Appendix A Calibration Procedure

This section it explained in details the device used, procedures for calibration, calibrations equations and a comparison between the not calibrated data vs. the calibrated data.

Report Document for the

High Accuracy Calibration Mechanism for Attitude Determination Systems

---

Prepared by:

Team Spokesperson (Jorge J. Quiñones) Date

Team Member (Javier Espinosa) Date

Revised:

Approved:

Institution Signoff (Dr. Hien Vo) Date

Inter-American University of Puerto Rico
Advance Research and Innovative Experience for students
(ARIES)

TABLE OF CONTENTS

Cover.....
Table of Contents.....

1.0 Document Purpose.....2-3
1.1 Document Scope.....2
1.2 Change Control and Update Procedures.....3

2.0 Reference Documents.....3-4

3.0 Tables of Figures.....5

4.0 Calibration Procedure .....…6-14

4.1 Calibration Procedure.....…….6-14
4.1.1 Accelerometer……8-9
4.1.2 Gyroscope……...10-11
4.1.3 Magnetometer…….12-13
4.2 Calibration Results…….....15-20

5.0 Acknowledgments.....21

6.0 Glossary 22

Inter-American University of Puerto Rico
Advance Research and Innovative Experience for students
(ARIES)

1.0 Document Purpose

This document describes the process of calibration using the High Accuracy Calibration Mechanism for Attitude Determination Systems.

1.1 Document Scope

This document specifies the Calibration of the sensors currently used on the HASP 2010 payload also provides the results of the calibration procedure. The document includes details of the calibration equations , procedure, performance, implementation and software develop.

1.2 Change Control and Update Procedures

Changes to this document shall only be made after approval by designated representatives from High Accuracy Calibration Mechanism for Attitude Determination Systems and the ARIES Institution Representative.

2.0 Reference Documents

Al-Nasir, J. (n.d.). *How does INS work?* Retrieved from http://www.al-nasir.com/www/Jamie/Articles/Technology/INS_Inertial_Navigation_explained.shtml

How Does an Accelerometer Work? (2011). Retrieved March 2011, from EzineArticles.com: http://ezinearticles.com/?How-does-an-Accelerometer-Work?&id=285604

Blue Point Engineering. (2007). *Servo Information.* Retrieved from http://www.bpesolutions.com/bpemanuals/Servo.Info.pdf

Central School for Tibetans. (2007). Retrieved from http://cstdalumni.org/invision-utilitech-3-non-ic-white-gimbal-recessed-kit/

CNCroutersource. (2007). *Open vs. Closed loop system.* Retrieved 2001, from http://www.cncroutersource.com/closed-loop-system.html

Coletta, V. (n.d.). College Physics.

King, A. (1998, November 13). *Inertial Navigation – Forty Years of Evolution.* Retrieved from http://www.imar-navigation.de/downloads/papers/inertial_navigation_introduction.pdf

MEMS Investor Journal, Inc. (2010). *MEMS BASED ATTITUDE AND HEADING REFERENCE SYSTEMS: OVERVIEW AND CURRENT TRENDS.* Retrieved from http://www.memsinvestorjournal.com/2010/12/mems-based-attitude-and-heading-reference-systems-overview-and-current-trends.html

NASA. (n.d.). *Earth's Inconstant Magnetic Field.* Retrieved from www.nasa.gov: http://science.nasa.gov/science-news/science-at-nasa/2003/29dec_magneticfield/

OPEN-LOOP CONTROL SYSTEM. (n.d.). Retrieved from http://www.tpub.com: http://www.tpub.com/content/neets/14187/css/14187_92.htm

O'Reilly, R., Harney, K., & Khenkin, A. (n.d.). *Sonic Nirvana: MEMS Accelerometers as Acoustic Pickups in Musical Instruments.* Retrieved from http://www.sensorsmag.com/sensors/acceleration-vibration/sonic-nirvana-mems-accelerometers-acoustic-pickups-musical-i-5852

pololu. (n.d.). *Micro Maestro 6-Channel USB Servo Controller* . Retrieved from http://www.pololu.com/catalog/product/1350

Robotzone, LLC. (1999). *Open loop vs closed loop control systems.* Retrieved from www.servocity.com: http://www.servocity.com/html/checkout.html

Robotzone. LLC. (n.d.). *What is a servo?* Retrieved from www.servocity.com: http://www.servocity.com/html/what_is_a_servo_.html

Sebastian, M. (n.d.). *Automated calibration of an accelerometers,.* Retrieved from http://www.x-io.co.uk/res/doc/automated_calibration_of_an_accelerometers_magnetometers_and_gyroscopes_a_feasibility_study.pdf

Senodia. (n.d.). *Working principle of MEMS gyro (Coriolis force).* Retrieved from http://senodia.com/english/products.php

Strickland, J. (n.d.). *What is a gimbal -- and what does it have to do with NASA?* Retrieved from howstuffworks.com: http://science.howstuffworks.com/gimbal1.htm

Watson Industries. (n.d.). *Attitude and Heading Reference System.* Retrieved from http://www.watson-gyro.com/products/attitude_reference_AHRS-S305_spec.html

what-when-how.com. (n.d.). *SPACECRAFT GUIDANCE, NAVIGATION AND CONTROL SYSTEMS.* Retrieved from http://what-when-how.com/space-science-and-technology/spacecraft-guidance-navigation-and-control-systems/

3.0 Table of Figures

FIGURE 1: HIGH ACCURACY CALIBRATION MECHANISM (HACM)..... 39
FIGURE 2: CALIBRATION ROUTINE PROGRAM AND GUI USING LABVIEW..... 39
FIGURE 3: ACCELEROMETER CALIBRATION ON Z AXIS. 40
FIGURE 4: ACCELEROMETER CALIBRATION FLOWCHART 41
FIGURE 5: GYROSCOPE FULL ROTATIONAL MOVEMENT FOR Z AXIS 43
FIGURE 6: GYROSCOPE CALIBRATION FLOWCHART..... 44
FIGURE 7: CALIBRATION MECHANISM WITH THE APPLIED MAGNET..... 46
FIGURE 8: MAGNETOMETER CALIBRATION FLOWCHART..... 47
FIGURE 9: EQUATIONS TO DETERMINE COEFFICIENTS A AND B..... 48
FIGURE 10: GYROSCOPE X AXIS CALIBRATED DATA VS RAW DATA..... 54
FIGURE 11: GYROSCOPE Y AXIS CALIBRATED DATA VS RAW DATA……..17
FIGURE 12: GYROSCOPE Z AXIS CALIBRATED DATA VS RAW DATA 56
FIGURE 16: ACCELEROMETER X AXIS CALIBRATED DATA VS RAW DATA 54
FIGURE 17: ACCELEROMETER Y AXIS CALIBRATED DATA VS RAW DATA 55
FIGURE 15: ACCELEROMETER Z AXIS CALIBRATED DATA VS RAW DATA 53
FIGURE 16: MAGNETOMETER Z AXIS CALIBRATED DATA VS RAW DATA 54
FIGURE 17: MAGNETOMETER X AXIS CALIBRATED DATA VS RAW DATA..... 55
FIGURE 18: MAGNETOMETER Y AXIS CALIBRATED DATA VS RAW DATA..... 56

4.0 Calibration Procedure

Calibration is the technique that involves the comparison of two or more measurements, which are analyzed and adjusted to determine estimated misalignment, bias, scale and obtain the values as close as possible to a known measurement of the device this guarantee a high accurate system. On IMU and AHRS devices the calibration procedure is very important, to be able to remove the systematic sensors errors. These errors can generate a notable gap between real and measured data reducing the system performance and accuracy. (Sebastian)

The Calibration of the sensors currently used on the HASP 2010 and 2011 payload was successfully performed for the following sensors accelerometer (SCA-3000) ,Gyroscope (ITG-3200) and Magnetometer(MicroMag3) . The calibration of the sensors was performed using the High Accuracy Calibration Mechanism (HACM) as illustrated in figure 1 , this calibration mechanism utilize three servo motors that can rotate the system with a closed-loop positional position feedback about ±180°, ±900°, and ±900° independently around the system pitch, roll and yaw axis respectively. The HACM is controlled using a pololu servo controlled that is interfaced to a computer through Labview. Since Labview provides a communication platform with the servo controller a calibration routine was performed using an algorithm as shown in figure 2.

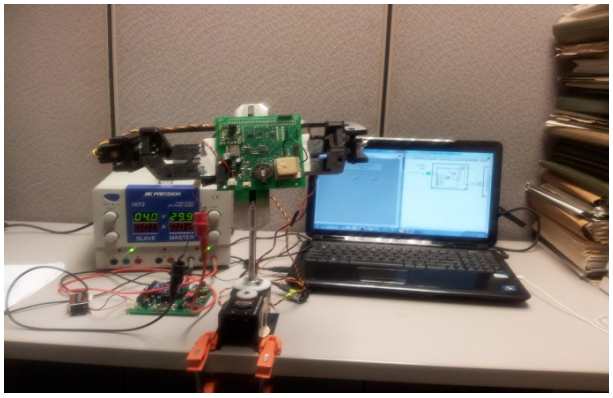

Figure 27: High Accuracy Calibration Mechanism (HACM)

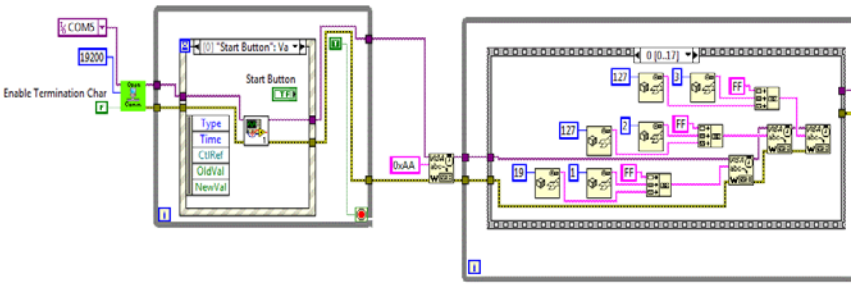

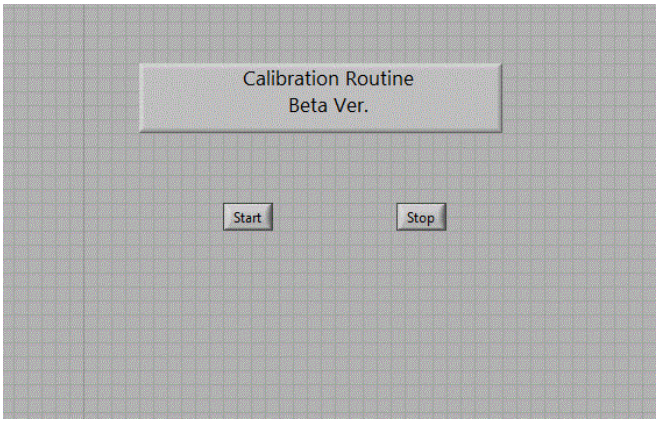

Figure 28: Calibration routine program and GUI using Labview

4.1.1 Accelerometer

To accomplish Accelerometer calibration is necessary to move the sensors through a range of orientations that are relative to the Earth's gravitational field, also the sensor must be able to rotate around its three axes (x, y, z) individually. During this action the data is collected at rate of 1 second per sample, on each orientation achieved through 180°steps over the full range of each axis. We can perform the calibration by simply letting the accelerometer static on a position with the chosen axis pointing up, you can assume that the vertical acceleration is 1G (where G is going to be the acceleration due to earth gravity). In the same way, if the chosen axis is pointing down then its acceleration should be -1G, and if is pointing horizontally then its acceleration should be zero.

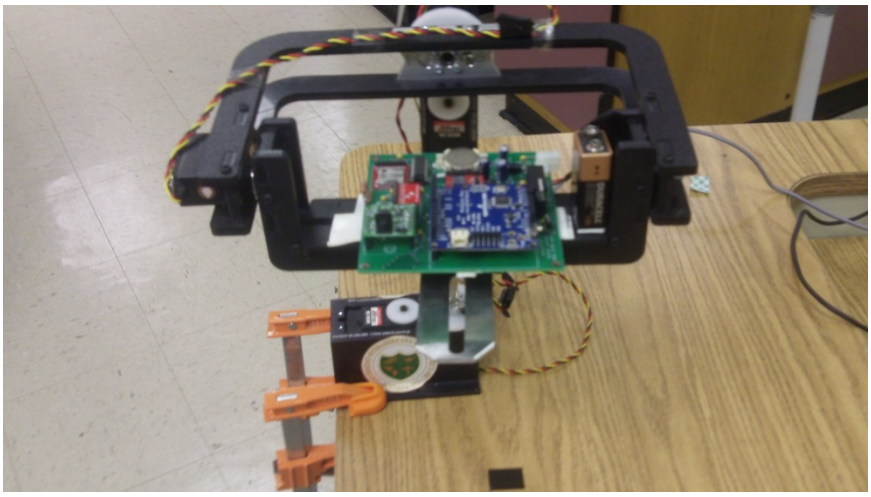

Figure 29: Accelerometer Calibration on Z axis.

Therefore since we have acquired *N* seconds of data, now we would have a series of acceleration measurements on that selected axis. So let's call this data value $X_{measured1}$, subsequently we applied a linear regression to that data to obtain a single value $x_{measured1}$ for this measurement step:

$x_{measured1}$ = Linear Regression ($X_{measured1}$)

Successively we repeat the same process for another known acceleration. This means that in our model, since the chosen axis was pointing up the first time around, we will now rotate the accelerometer so that the chosen axis points on the opposite direction.

Performing this for every axis gather enough information to construct a table:

	real	measured
1st measurement	X_{real1} (1G)	$x_{measured1}$
2nd measurement	X_{real2} (-1G)	$-x_{measured2}$

And so we can calculate A and B by simply solving the system:

$$X_{real1} = A\, x_{measured1} + B$$
$$x_{real2} = A\, x_{measured2} + B$$

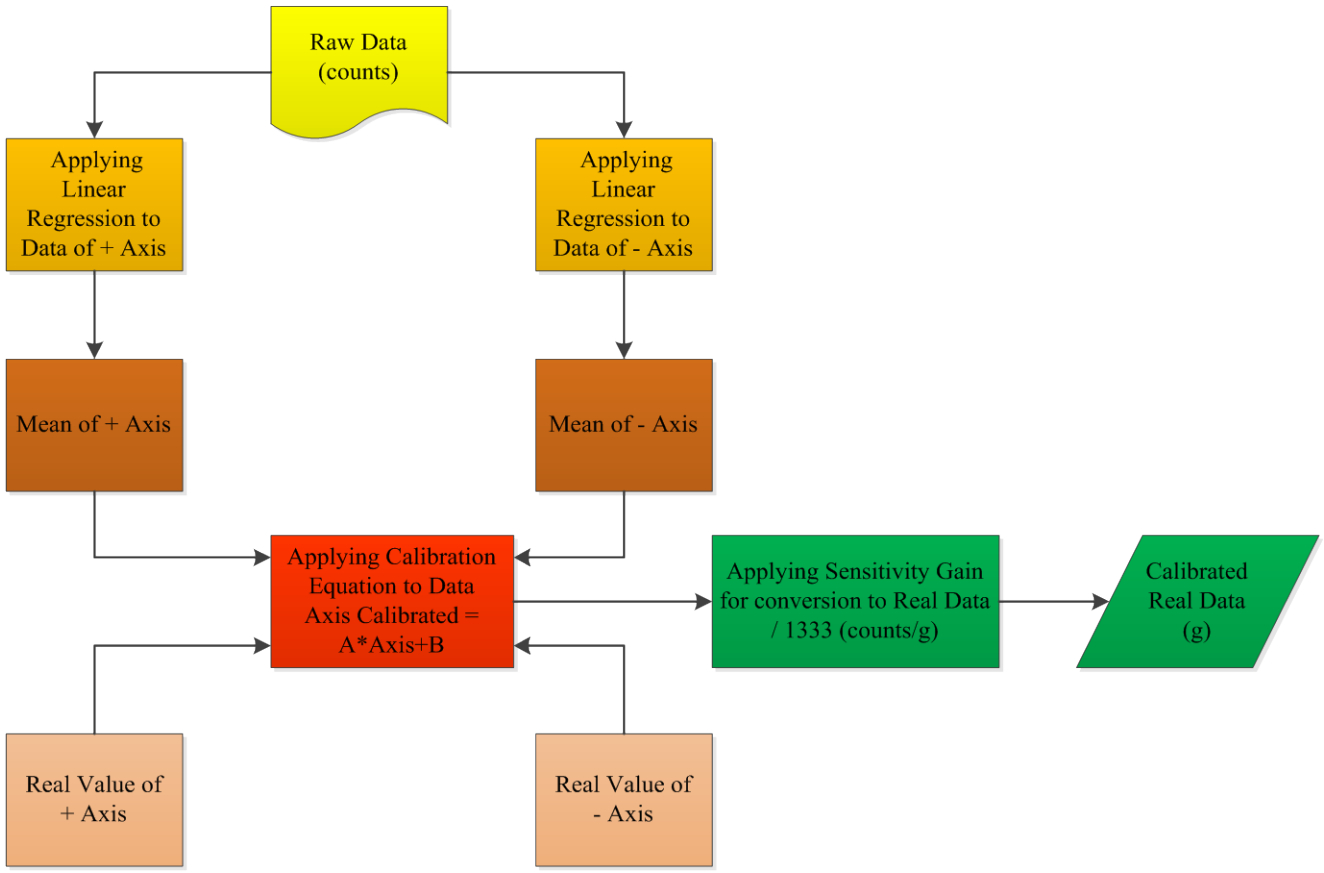

Figure 30: Accelerometer Calibration Flowchart

Inter-American University of Puerto Rico
Advance Research and Innovative Experience for students
(ARIES)

4.1.2 Gyroscope

For the calibration procedure of the gyroscope it's necessary to rotate around one axis by a known angular velocity and ensures that the angular velocity measured by the gyroscope is equal to the known angular velocity . Then be repeated for all three axes (x, y, z). To achieve an accurate calibration, the program collects each gyroscope axis calibration dataset at 1 sample by second during a full rotation around each axis at a constant angular velocity for nearly five minutes. The constant angular velocity is determine by recording the rotation of the HACM using a High Definition camera and performing a video analysis using a professional video editing software.

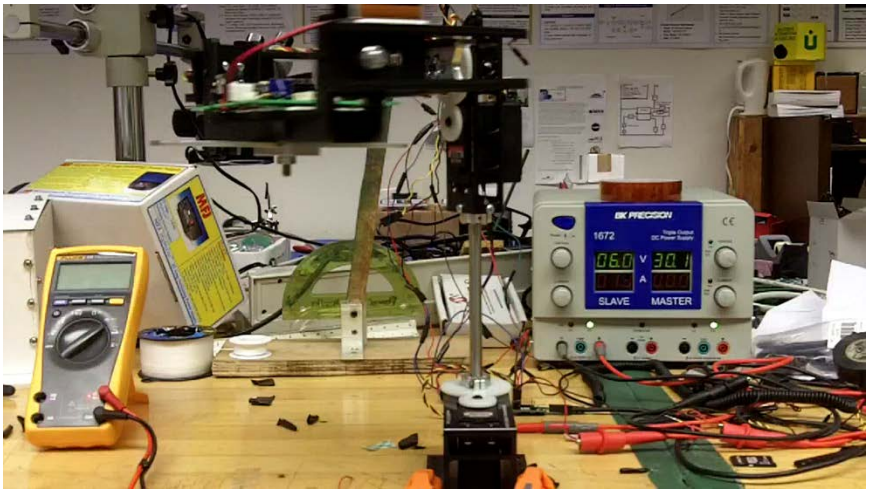

Figure 31: Gyroscope full rotational movement for Z axis

Since we have the constant angular velocities exerted we proceed to repeat the steps used for the accelerometer but for different known rotation speeds instead of different orientations of the sensor. Finally all the data obtained from the sensors throughout the calibration procedure its stored on the SD card to perform the calibration calculations.

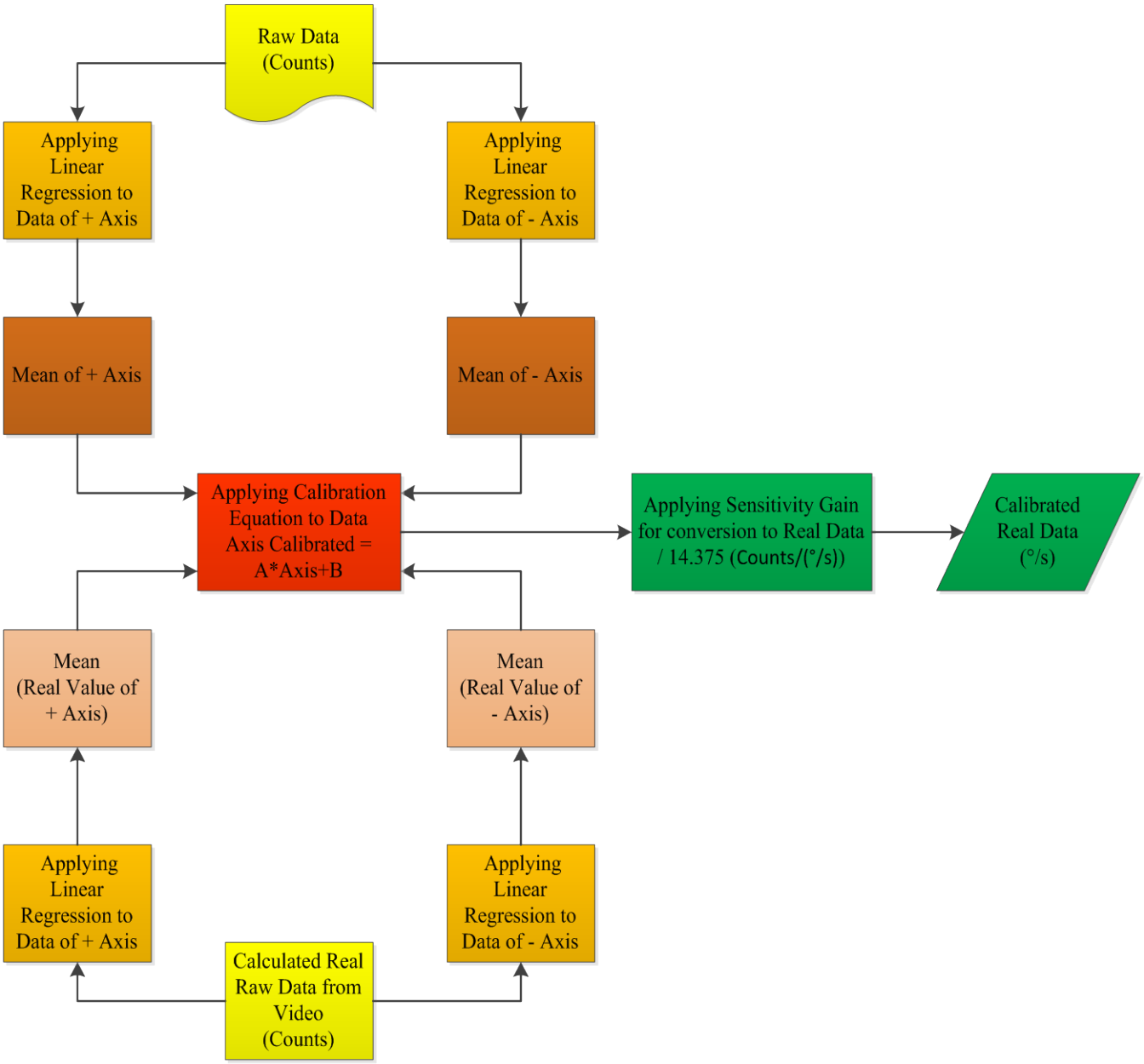

Figure 32: Gyroscope Calibration Flowchart

4.1.3 Magnetometer

The magnetometer measurements of the magnetic are usually corrupted by numerous errors including sensor manufacture problems , noise and magnetic deviations induced by electronic equipment, metals and other errors.

To perform the calibration for the magnetometer was necessary to figured out a way to have a known magnetic field value. In that way we can used the same process performed for the accelerometer and gyroscope. This is basically impossible if you don't have access to this type of equipment. For that reason we choose to utilize a speaker magnet to approximately determine the real value of the magnetic field measured by the sensor.

To be able to calculate the magnet field we develop an experiment consisting on gathering data in all three axes (x, y, z) of the magnetometer, then we repeat the process but with the magnet applied. The magnet its applied aligned with z axis and remain at the same position for each orientation as show in figure 7 we only vary the direction of the axis, positive or negative, so we can assumed a constant applied magnetic force in the selected direction.

Then to determine the value of the magnetic field produced by the magnet, we calculate the difference between the raw data with applied magnet and the raw data alone. This operation only produce one value for the axis, positive or negative , since we only have one value its necessary to do the same process for the other component of the same axis.

Therefore performing an average calculation between positive and negative values we can determine approximately the average value of the magnetic field intensity at the selected axis.

Since we have the approximately value of the magnetic field exerted to the axis, now we need to find the real value of the magnetic field on the axis. Therefore its necessary to take the Raw data with the magnet applied and subtract the value of the average magnetic field. Performing this action generates our "Real "value of the calibration equation. Now we can used the same steps employed for the accelerometer to calibrate the magnetometer.

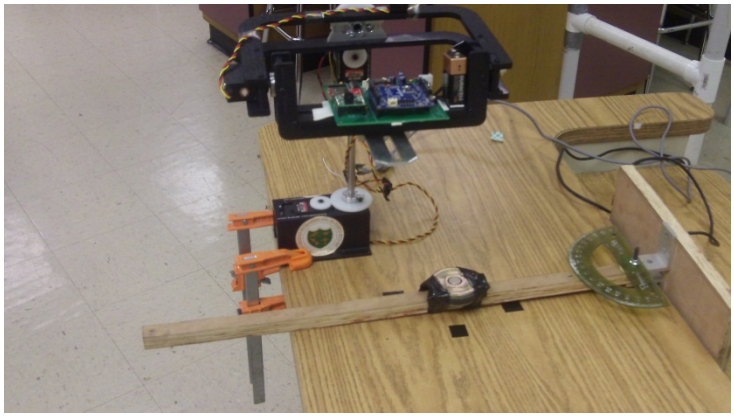

Figure 33: Calibration Mechanism with the applied magnet

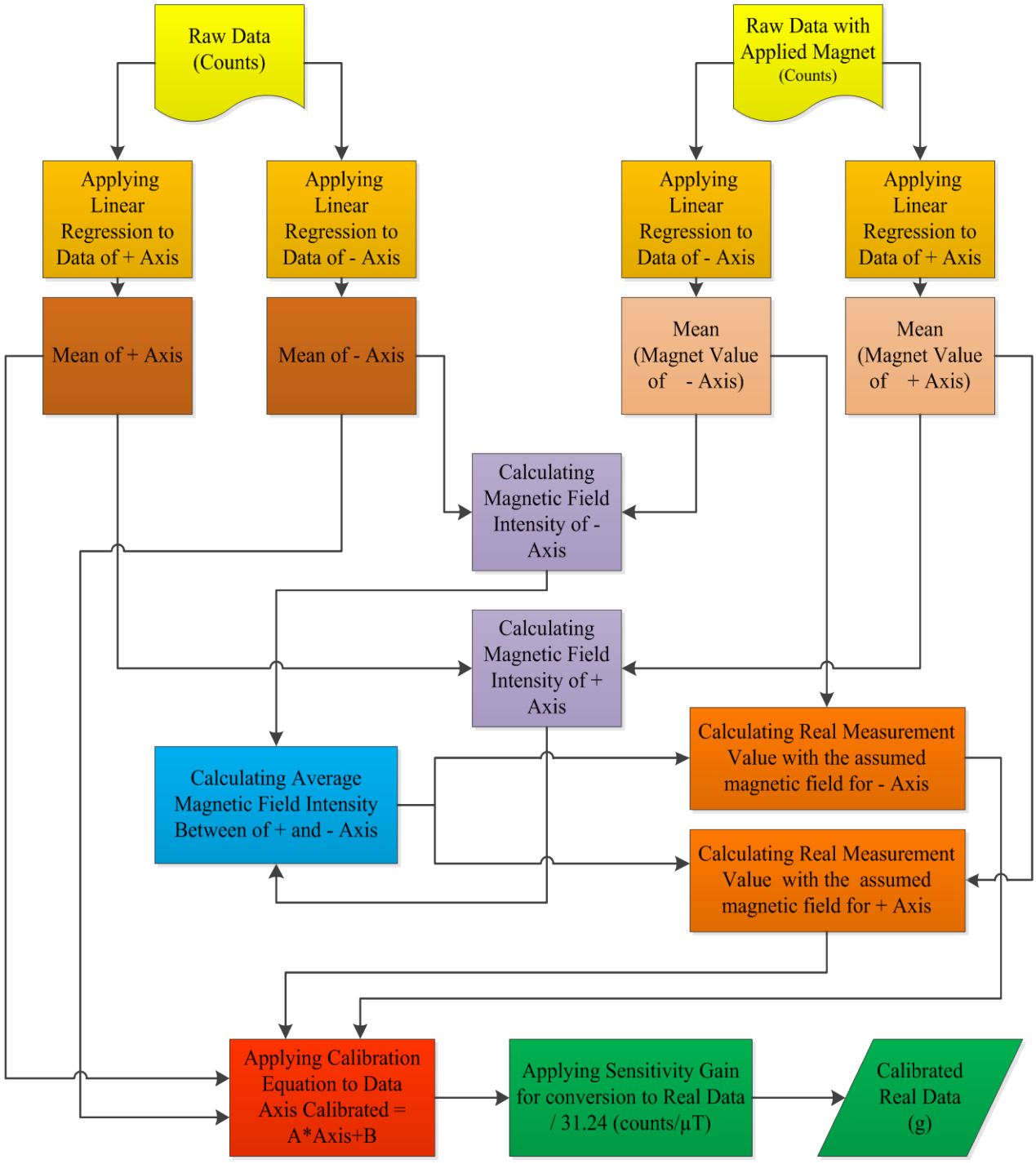

Figure 34: Magnetometer Calibration Flowchart

Assuming that the output responses of the sensors are linear with respect to the real value that they are measuring, means that the calibration equation is the same as finding the parameters A and B in the equations below:

$$xreal1 = A\,xmeasured1 + B$$

$$xreal2 = A\,xmeasured2 + B$$

Where $xreal1$ and $xreal2$ are the knowing quantities that are used as reference to established the equation.

The $xmeasured1$ and $xmeasured2$ are the real value obtained from the sensors and are calculated by performing a linear Regression of the gather data.

The A and B are the two unknowns of the equations. Now by simply solving for A and B we get:

$$B = x_{real1} - A \cdot x_{measured1}$$

$$x_{real2} = A \cdot x_{measured2} + \left(x_{real1} - A \cdot x_{measured1}\right)$$
$$x_{real2} - x_{real1} = A \cdot \left(x_{measured2} - x_{measured1}\right)$$
$$A = \frac{x_{real2} - x_{real1}}{x_{measured2} - x_{measured1}}$$
$$B = x_{real1} - \left(\frac{x_{real2} - x_{real1}}{x_{measured2} - x_{measured1}}\right) \cdot x_{measured1}$$

Figure 35: Equations to determine coefficients A and B

Now with the values of *A* and *B* for each component. Then is simply to use the calibration equation to obtain calibrated values from the measurements.

Implementation of this equation was performed during the post flight analyze of the data on Dspic33 and arduino obtaining successfully results.

4.4 Calibration Results:

This section describes the results obtained through the calibration process performed to the HASP sensors. This calibration procedure generates the following equations for each sensor axis.

Gyroscope

Calibrations results for Gyroscope using the following calculated equations for each axis:

$$X_{axis\ calibrated} = 1.0443 * X_{axismeasured} + 2.44732$$

$$Y_{axis\ calibrated} = .9744 * Y_{axismeasured} - .5610$$

$$Z_{axis\ calibrated} = .9962 * Z_{axismeasured} - .588447$$

Applying this equation directly to the code on the arduino or dsPIC33 microcontroller would display the calibrated data in real time, but to accomplish the analysis these equation were applied to the data stored in the sdcard that contain the HASP flight .Applying these calculation generates the following result:

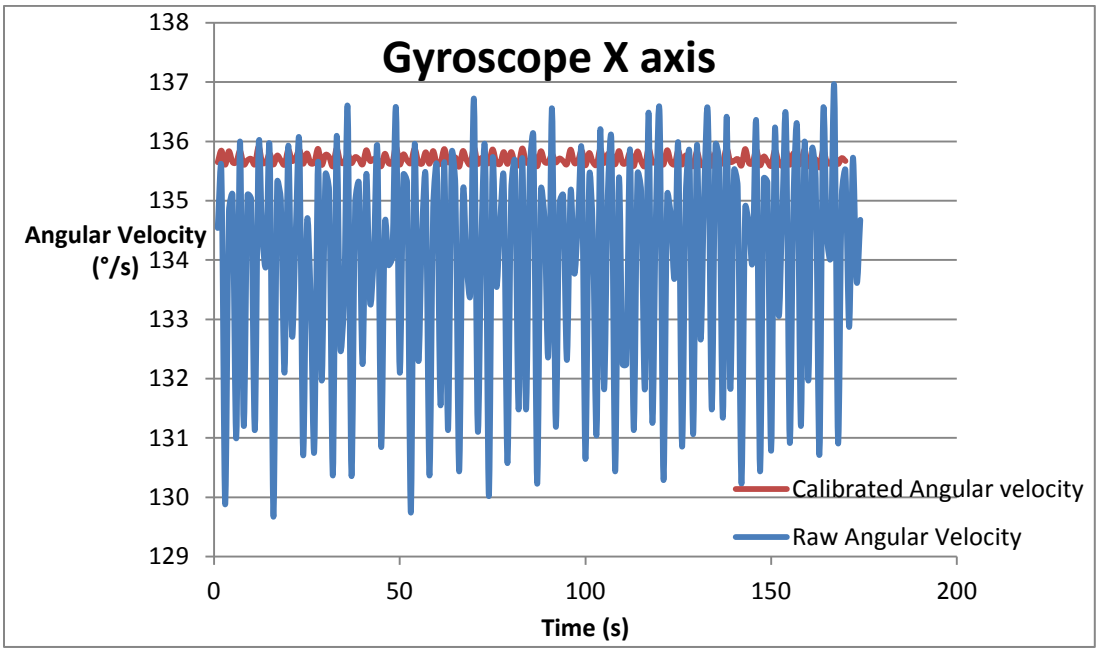

Figure 10: Gyroscope X axis Calibrated data vs Raw data

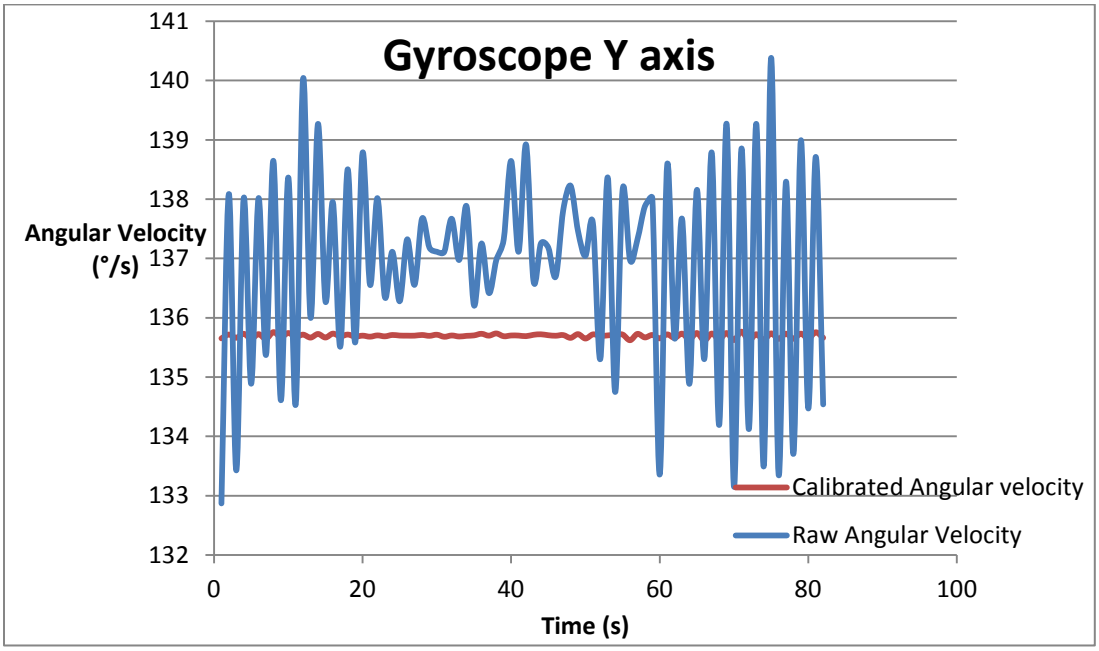

Figure 11: Gyroscope Y axis Calibrated data vs Raw data

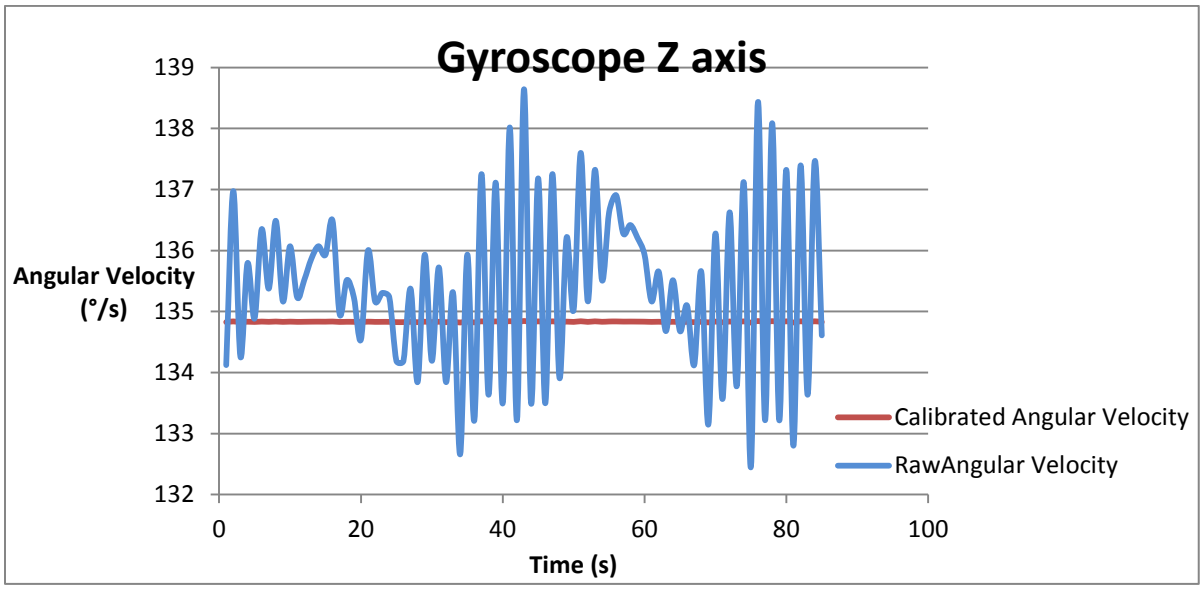

Figure 12: Gyroscope Z axis Calibrated data vs Raw data

The data of the angular velocity obtained during the calibration process for the gyroscope three axes as shows in **Figure 10,11,12** demonstrated the difference between raw data (red) and the calibrated (blue). The first data obtained (raw) contain a lot of noise , high fluctuations and errors in the values that needs to be corrected, filtered and calibrated to obtain an accurate real value. Throughout the execution of this calibration we can obtain a new data (calibrated) that is much more precise in comparison with the raw data as illustrate **Figure 10, 11,12**.

Accelerometer

Calibrations results for accelerometer using the following calculated equations:

$$X_{axis\ calibrated} = 1.0032 * X_{axismeasured} + .02066$$

$$Y_{axis\ calibrated} = 1.0278 * Y_{axismeasured} - .0659$$

$$Z_{axis\ calibrated} = 1.0119 * Z_{axismeasured} - .0243$$

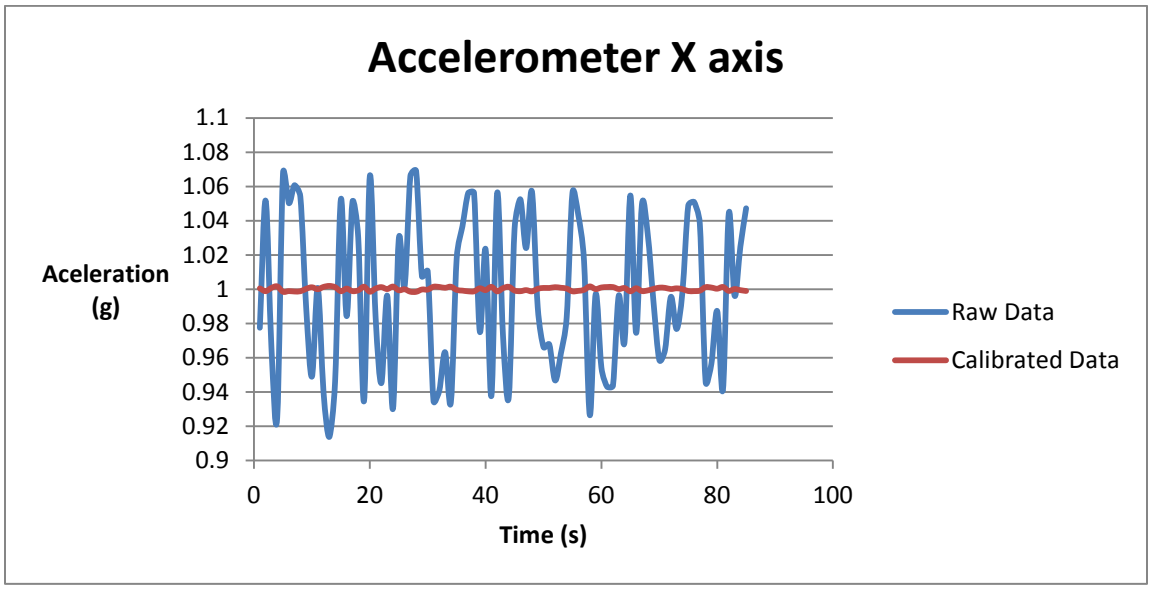

Figure 13: Accelerometer X axis Calibrated data vs Raw data

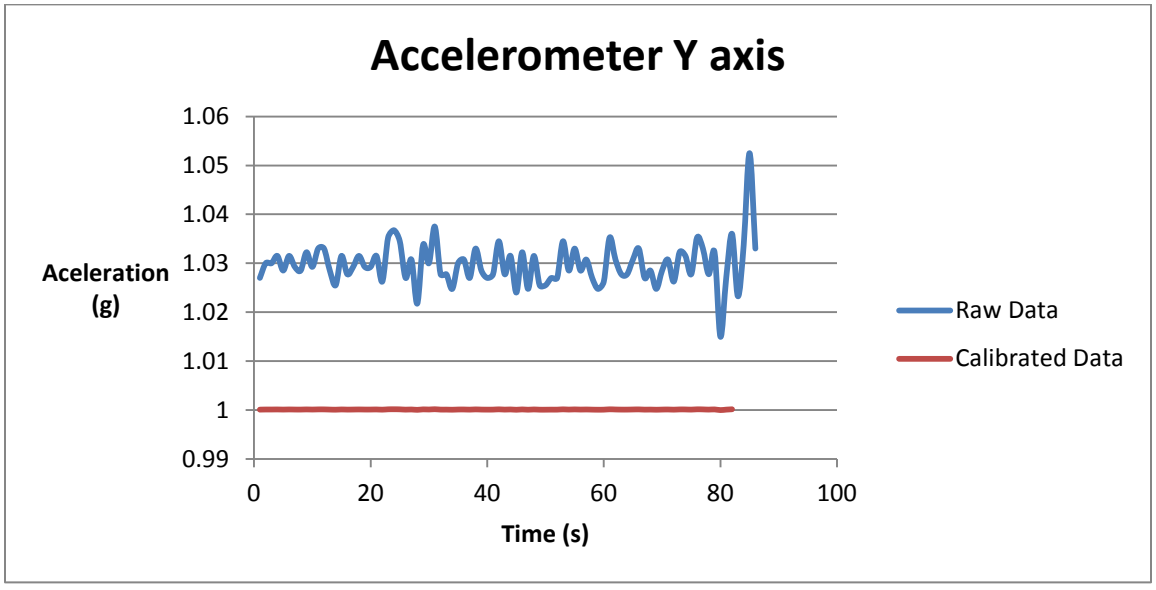

Figure 14: Accelerometer Y axis Calibrated data vs Raw data

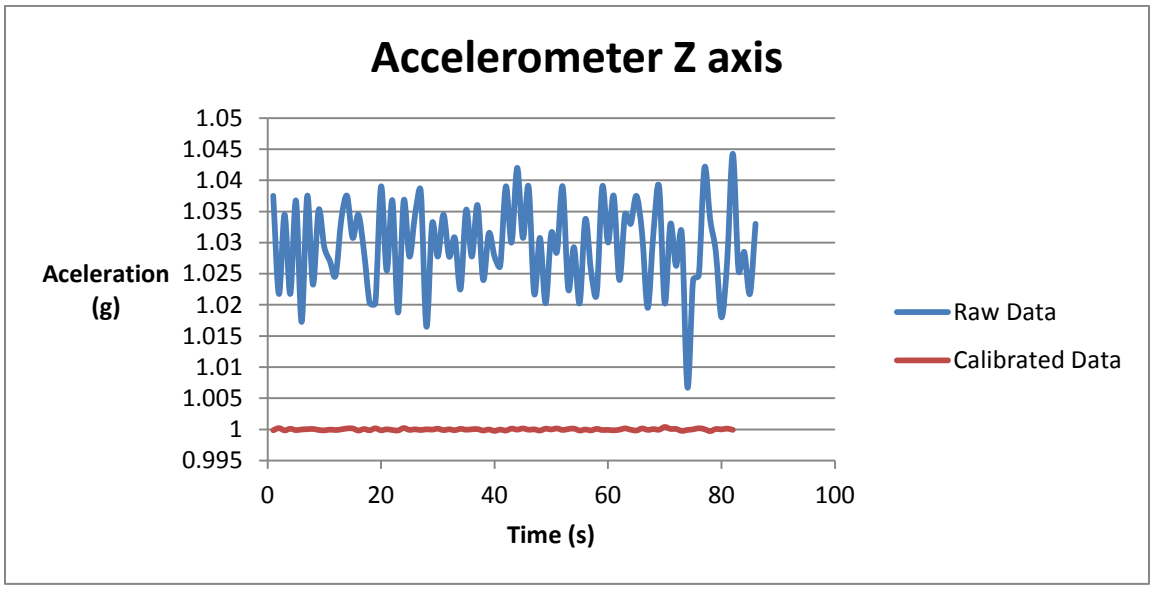

Figure 36: Accelerometer Z axis Calibrated data vs Raw data

The three axes accelerometer data illustrated in **Figure 13, 14, 15** demonstrate the behavior during the flight on the HASP .The data gathered from the accelerometer shows very low fluctuations but some noise in the measure represented with the blue line. Throughout the calibration process of the accelerometer data we manage to attenuate the noise and reduce the fluctuations of the values.

Magnetometer

Calibrations results for Magnetometer using the following calculated equations:

$$X_{axis\ calibrated} = (.9999 * X_{axismeasured\ raw} + 28.97)/31.45$$

$$Y_{axis\ calibrated} = (1.0000 * Y_{axismeasured\ raw} - 313.9050)/31.45$$

$$Z_{axis\ calibrated} = (1.0000 * Z_{axismeasured\ raw} - 98.00)/31.45$$

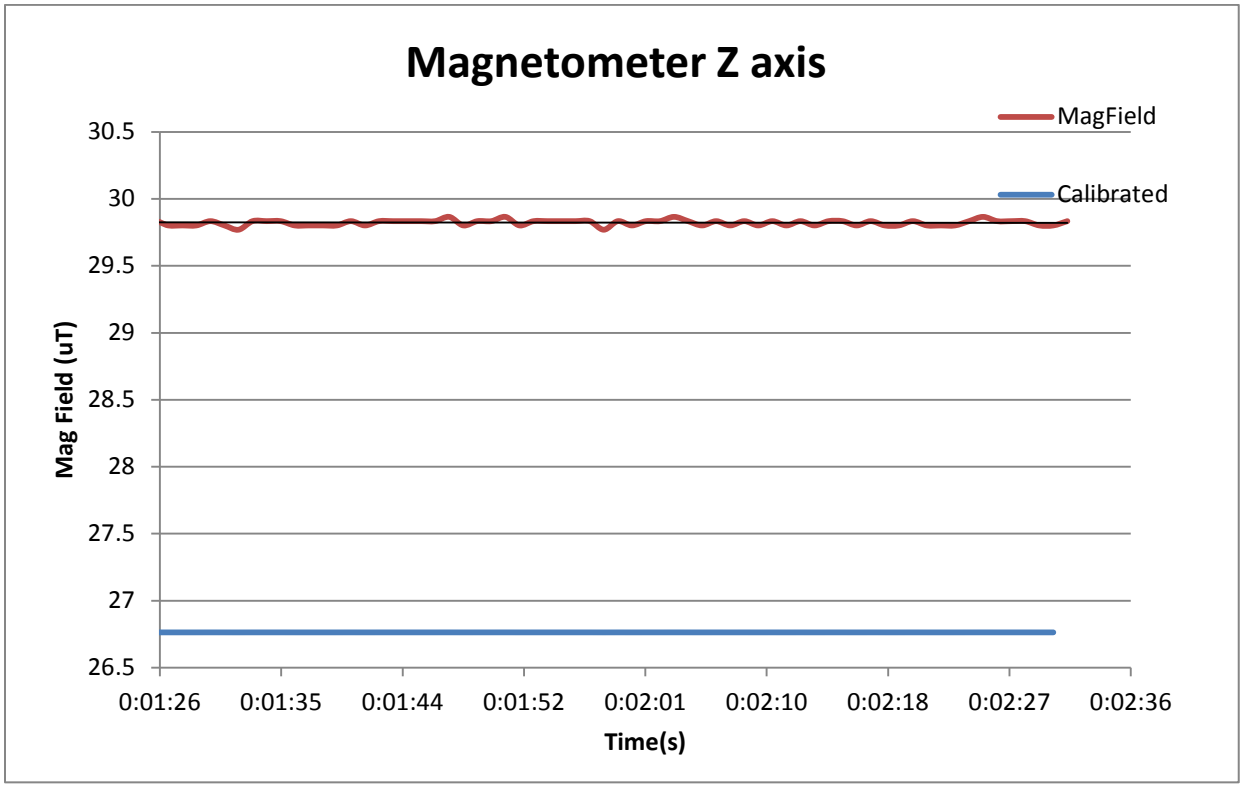

Figure 37: Magnetometer Z axis Calibrated data vs Raw data

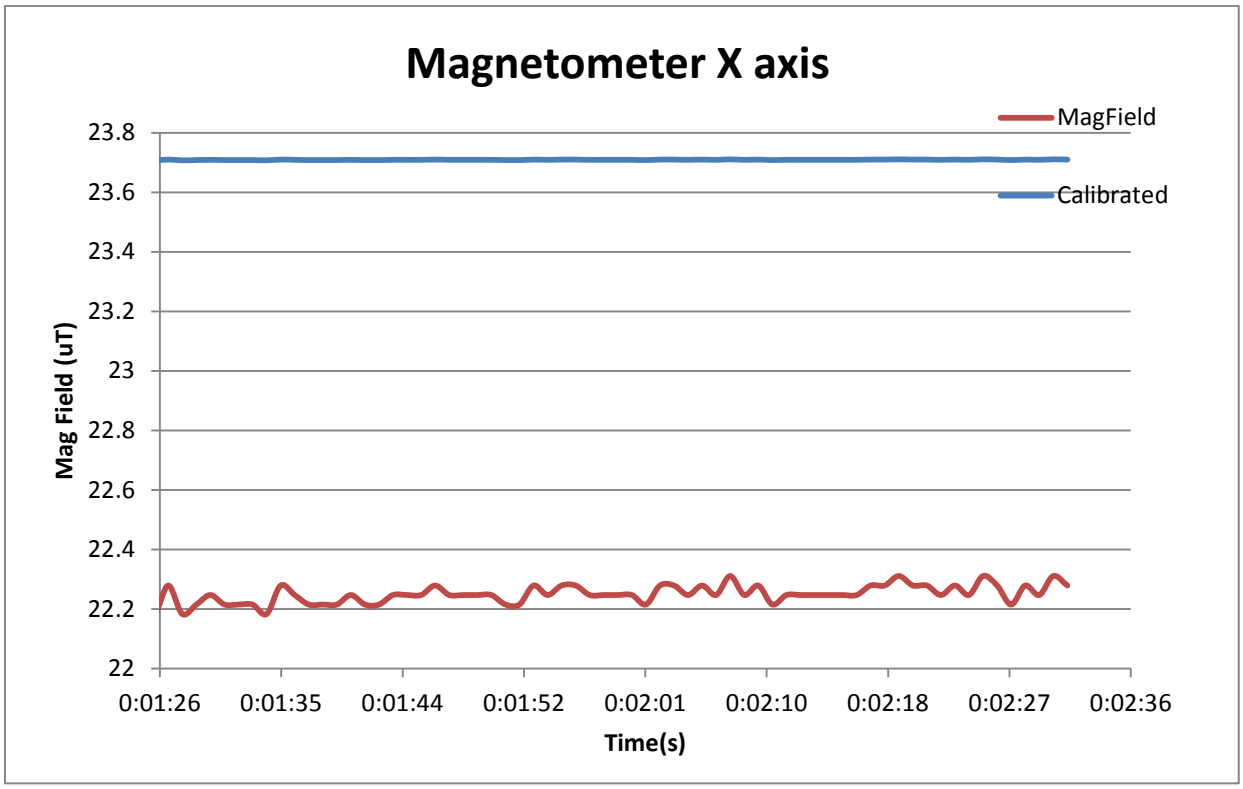

Figure 38: Magnetometer X axis Calibrated data vs Raw data

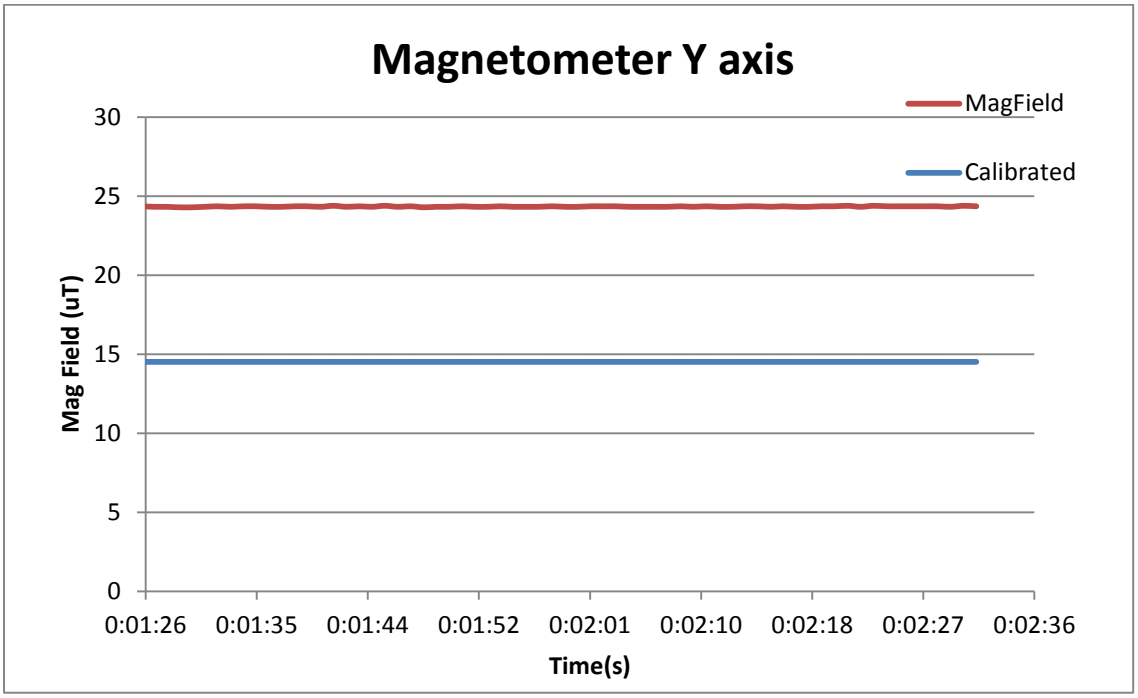

Figure 39: Magnetometer Y axis Calibrated data vs Raw data

The data gathered from the magnetometer present the most inaccuracy between raw data and calibrated . This due to the nonexistence of necessary equipment to perform the magnetometer calibration in the best possible way. To be able to obtain an accurate data it is necessary a Helmholtz coil that can generate the know magnetics fields necessary to perform a more accurate calibration. Never less the calibration performed using the available equipment produced the results show in **Figure 16, 17, 18 .** These results demonstrate the performance of the calibration, that manage to reduce the noise of the measures but were unable to decrease the fluctuation between values due the calibration equations obtained with the data used. However to achieve a better performance in the future we need to update the equations and apply again to raw data.

5.0 Acknowledgments

This project was accomplished thanks to the help of the following people:

- Dr. Hien Vo, Principal Investigator, UIPR- Bayamón
- Dr.Pedro Capo Lugo, NASA Engineer, NASA Marshall Space Flight Center
- Jose Molina, Graduated Computer Engineering Student, UIPR-Bayamón
- Abel Torres, Undergraduate Computer Engineering Student
- Edwin Pagán, Undergraduate Electrical Engineering Student , UIPR-Bayamón
- Janice Longoria, Undergraduate Mechanical Engineering Student , UIPR-Bayamón
- Ana Espinal , Graduate Electrical Engineering Student , UIPR-Bayamón
- VECTOR Team, Undergraduate Engineering Students , UIPR-Bayamón

6.0 Glossary

LAACES	Physics & Aerospace Catalyst Experiences in Research
GUI	Graphical User Interface
AHRS	Attitude Heading Reference System
MEMS	Micro Electrical Mechanical System
TBD	To be determined
TBS	To be supplied
IMU	Inertial Measurement Unit
INS	Inertial Navigation System
SINS	Strapdown Inertial Navigation System
Gyro	Gyroscope
PWM	Pulse Width Modulation